iScience

CellPress
OPEN ACCESS

Article

Biofabrication of synthetic human liver tissue with advanced programmable functions

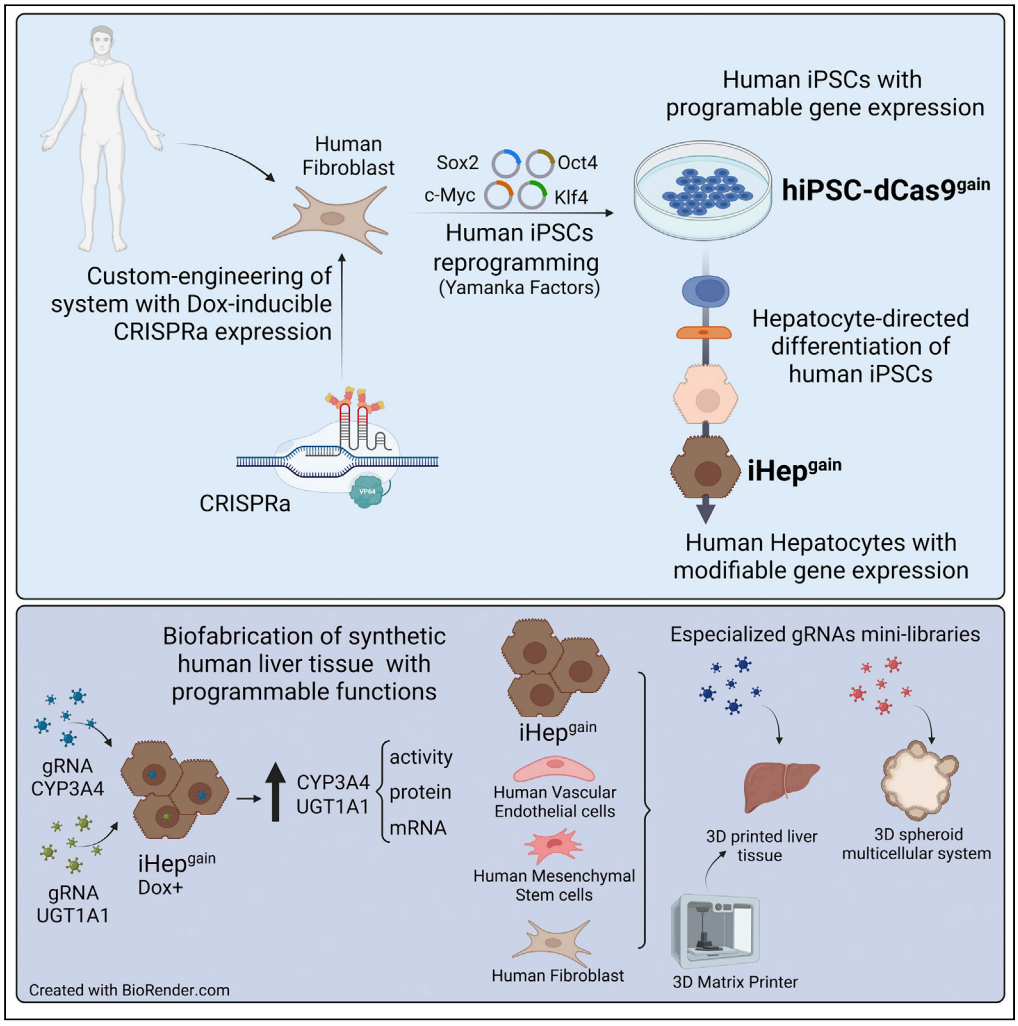

Rodrigo M. Florentino, Kazutoyo Morita, Nils Haep, ..., D. Lansing Taylor, Ira J. Fox, Alejandro Soto-Gutierrez

als208@pitt.edu

Highlights

Edited human iPSCs^{gain} can control transcriptional activation

CYP3A4 and UGT1A1 activity in human iHeps^{gain} are similar to human hepatocytes

Human iHeps^{gain} generate synthetic liver tissue with advanced programmable functions

Florentino et al., iScience 25, 105503
December 22, 2022
https://doi.org/10.1016/j.isci.2022.105503

iScience

CellPress
OPEN ACCESS

Article

Biofabrication of synthetic human liver tissue with advanced programmable functions

Rodrigo M. Florentino,[1,2,9] Kazutoyo Morita,[1,9] Nils Haep,[1,9] Takashi Motomura,[1] Ricardo Diaz-Aragon,[1] Lanuza A.P. Faccioli,[1] Alexandra Collin de l'Hortet,[1] Zeliha Cetin,[1] Carla Frau,[1] Lawrence Vernetti,[2,3,4] Anna-Klara Amler,[5] Alexander Thomas,[5] Tobias Lam,[5] Lutz Kloke,[5] Kazuki Takeishi,[1,6] D. Lansing Taylor,[2,3,4] Ira J. Fox,[4,7,8] and Alejandro Soto-Gutierrez[1,2,3,8,10,*]

SUMMARY

Advances in cellular engineering, as well as gene, and cell therapy, may be used to produce human tissues with programmable genetically enhanced functions designed to model and/or treat specific diseases. Fabrication of synthetic human liver tissue with these programmable functions has not been described. By generating human iPSCs with target gene expression controlled by a guide RNA-directed CRISPR-Cas9 synergistic-activation-mediator, we produced synthetic human liver tissues with programmable functions. Such iPSCs were guide-RNA-treated to enhance expression of the clinically relevant CYP3A4 and UGT1A1 genes, and after hepatocyte-directed differentiation, cells demonstrated enhanced functions compared to those found in primary human hepatocytes. We then generated human liver tissue with these synthetic human iPSC-derived hepatocytes (iHeps) and other non-parenchymal cells demonstrating advanced programmable functions. Fabrication of synthetic human liver tissue with modifiable functional genetic programs may be a useful tool for drug discovery, investigating biology, and potentially creating bioengineered organs with specialized functions.

INTRODUCTION

Liver failure causes more than 30,000 deaths per year in the US alone. Aggressive clinical management can extend life, but the only definitive therapy for end-stage liver disease is allogeneic orthotopic liver transplantation.[1,2] Widespread use of liver transplantation is limited by a shortage of donor organs,[3] primary graft dysfunction,[4] the need for long-term immune suppression, and high cost.[5] Many strategies are being explored to increase the availability of donor livers, including resuscitation of marginal-quality livers by machine perfusion[6] and transplantation of livers from non-human donors, such as the pig,[7] all of which currently have various technical and practical difficulties. As the liver can regenerate even after severe injury, temporary hepatic support is beneficial in some circumstances.[8] The ability to engineer livers from autologous cells such as patient-derived induced pluripotent stem cells might ultimately provide transplantable organs and eliminate the need for life-long immune suppression.[9] However, liver tissue engineered in this way has produced limited clinically relevant functions.

Use of programmable DNA-binding proteins, such as CRISPR-Cas9, has revolutionized genome modulation and has been used as a platform for modulating endogenous gene expression.[10–13] The catalytically deficient, Cas9 synergistic activation mediator (dCas9-SAM) system[10] is an engineered protein complex used for transcriptional activation of endogenous genes, where it has been shown to be highly efficient at activating gene expression and function when compared to other systems.[14]

We have previously generated protocols for differentiating human-induced pluripotent stem cells (hiPSCs) into hepatocyte and other liver non-parenchymal cells,[9,15] and have now created hiPSCs with programmable expression of specific genes based on use of the dCas9-SAM system. Following differentiation of these cells into human iPS-derived hepatocytes (iHeps), we examined the extent of hepatic gene activation in a guide RNA (gRNA)-dependent manner. We demonstrated stable programmable expression derived from the dCas9-SAM system in human iPSCs (Human iPSCs-Cas9^{gain}) at any stage of hepatocyte-directed

[1]Department of Pathology, University of Pittsburgh, Pittsburgh, PA, USA

[2]Pittsburgh Liver Research Center, University of Pittsburgh, Pittsburgh, PA, USA

[3]University of Pittsburgh Drug Discovery Institute, University of Pittsburgh, Pittsburgh, PA, USA

[4]Department of Computational and Systems Biology, University of Pittsburgh, Pittsburgh, PA, USA

[5]Cellbricks GmbH, Gustav-Meyer-Allee 25, 13355 Berlin, Germany

[6]Department of Surgery and Science, Graduate School of Medical Sciences, Kyushu University, Fukuoka, Japan

[7]Department of Surgery, Children's Hospital of Pittsburgh of UPMC, University of Pittsburgh, Pittsburgh, PA, USA

[8]McGowan Institute for Regenerative Medicine, University of Pittsburgh, Pittsburgh, PA, USA

[9]These authors contributed equally

[10]Lead contact

*Correspondence: als208@pitt.edu

https://doi.org/10.1016/j.isci.2022.105503

differentiation. As proof of principle, we selected two genes, CYP3A4 and UGT1A1, normally expressed only by mature human hepatocytes, but poorly expressed in iPSC-derived hepatocytes to test the synergistic activation mediator system. By delivering gRNAs for these two genes into human iHeps^{gain}, we found that mRNA and protein expression of CYP3A4 and UGT1A1 were specifically upregulated and functional activity to the level found in freshly isolated human hepatocytes in both 2D and 3D liver tissue configurations. Therefore, we believe that biofabrication of synthetic human liver tissue with advanced programmable functions could represent a viable approach to interrogate maturation mechanisms and functions.

RESULTS

Establishment of human fibroblasts with inducible dCas9 and a gene expression activator system

CRISPR-Cas9 is a simple and efficient tool for genome editing and has enabled genome-wide CRISPR screens in mice and cell lines.[16–19] We, therefore, sought to generate human iPSCs with inducible dCas9 expression. We first transduced human primary fibroblasts (HF) with Tet-on-3G doxycycline (Dox)-inducible lentiviral vectors containing inducible dCas9^{gain} (dCas9-VP64 and the synergistic activation mediator (SAM) system) (neomycin resistant) and inducible SAM containing GFP (puromycin resistant) (Figure 1A). After neomycin and puromycin selection, the transduced fibroblasts (HF-dCas9^{gain}) exhibited a Dox-dependent 28-fold Tet-On-3G induction of Cas9 (*p = 0.0168 in mRNA) and a 62.5-fold induction of SAM (*p = 0.0394) as assessed by mRNA and GFP expression (Figure 1A).

Generation of human iPSCs from edited fibroblasts carry programmable Cas9-gain-of-function

The stably transduced human fibroblast (HF-dCas9^{gain}) was then programmed into iPSCs as described.[20] The resulting human iPSC colonies showed, by mRNA and protein production, high expression of inducible dCas9^{gain} and SAM-GFP after Dox exposure. The resulting human iPSCs were cultured for >10 passages in the presence of neomycin and puromycin for enrichment and stability. We named these cells "human iPSCs-dCas9^{gain}". The human iPSCs-Cas9^{gain} showed a 15-fold induction of Cas9 ($p < 0.0001$ in mRNA) and 322.5-fold ($p = 0.0087$ in mRNA) induction of SAM-GFP after Dox exposure, as assessed by mRNA and protein expression for either dCas9 or GFP (Figure 1B).

Human iPSCs-dCas9^{gain} showed normal pluripotent morphology, consisting of compact colonies with distinct borders similar to that seen in human embryonic stem cells (hESCs),[21] expressed NANOG, OCT4, TRA-1-60, and SSEA4 (Figure 1C) and displayed uniform mRNA expression of pluripotency markers (C-Myc, Lin28, SOX2, Nanog, and Oct3/4) comparable to that seen in human iPSCs (WTC-11) (Figures 1C and S1). The cells also had a normal karyotype (Figure 1D). Embryoid bodies derived from human iPSCs-Cas9^{gain} spontaneously expressed ectodermal (SOX1 and Otx-2), mesodermal (Brachyury and HAND1), and endodermal (GATA-4 and SOX17) markers (Figure 1E). Thus, engineering of human iPSCs-Cas9^{gain} did not affect pluripotency or produce chromosomal alterations. Finally, the human iPSCs-dCas9^{gain} were tested for the presence or absence of three single nucleotide polymorphisms that could affect hepatic differentiation and/or function[22]: PNPLA3 (rs738409C>G) MBOAT7/TMC4 (rs641738C>T) and GCKR (rs780094C>T). Human iPSCs-Cas9^{gain} were "heterozygous" for the PNPLA3 C allele, had a "normal" C/C MBOAT7 allele, and were "heterozygous" for the GCKR C allele (Figure 1F).

Hepatocyte-directed differentiation of gene programmable human iPSCs

We then differentiated the human iPSCs-dCas9^{gain} toward hepatocytes using our previously published protocol[9,15,23,24] with modifications. Cells were first cultured in monolayers with a combination of activin A, bone morphogenetic protein 4 (BMP4), and fibroblast growth factor (FGF)-2 to induce definitive endoderm (Stage 1&2) (Figure 2A). Greater than 80% of cells expressed the definitive endoderm markers SOX17 (Figure 2B) and CXC chemokine receptor 4 (CXCR4; Figure 2C) at day 4. Then, cells were cultured for 14 days in the presence of dimethyl sulfoxide (DMSO) and human hepatocyte growth factor (hHGF) to induce hepatocyte specificity (Stage 3). Finally, cells were cultured for 4 additional days in DMSO and HGF with low glucose in the presence of endodermal growth factor, dexamethasone, hydrocortisone, free fatty acids, bile acids, and cholesterol (Figure 2A)(Stage 4) to induce hepatic maturation.

To determine the time course and extent to which human iPSCs-dCas9^{gain} cells were differentiated into hepatocytes, immunostaining was performed for albumin (ALB) and α-fetoprotein (AFP), and the adult

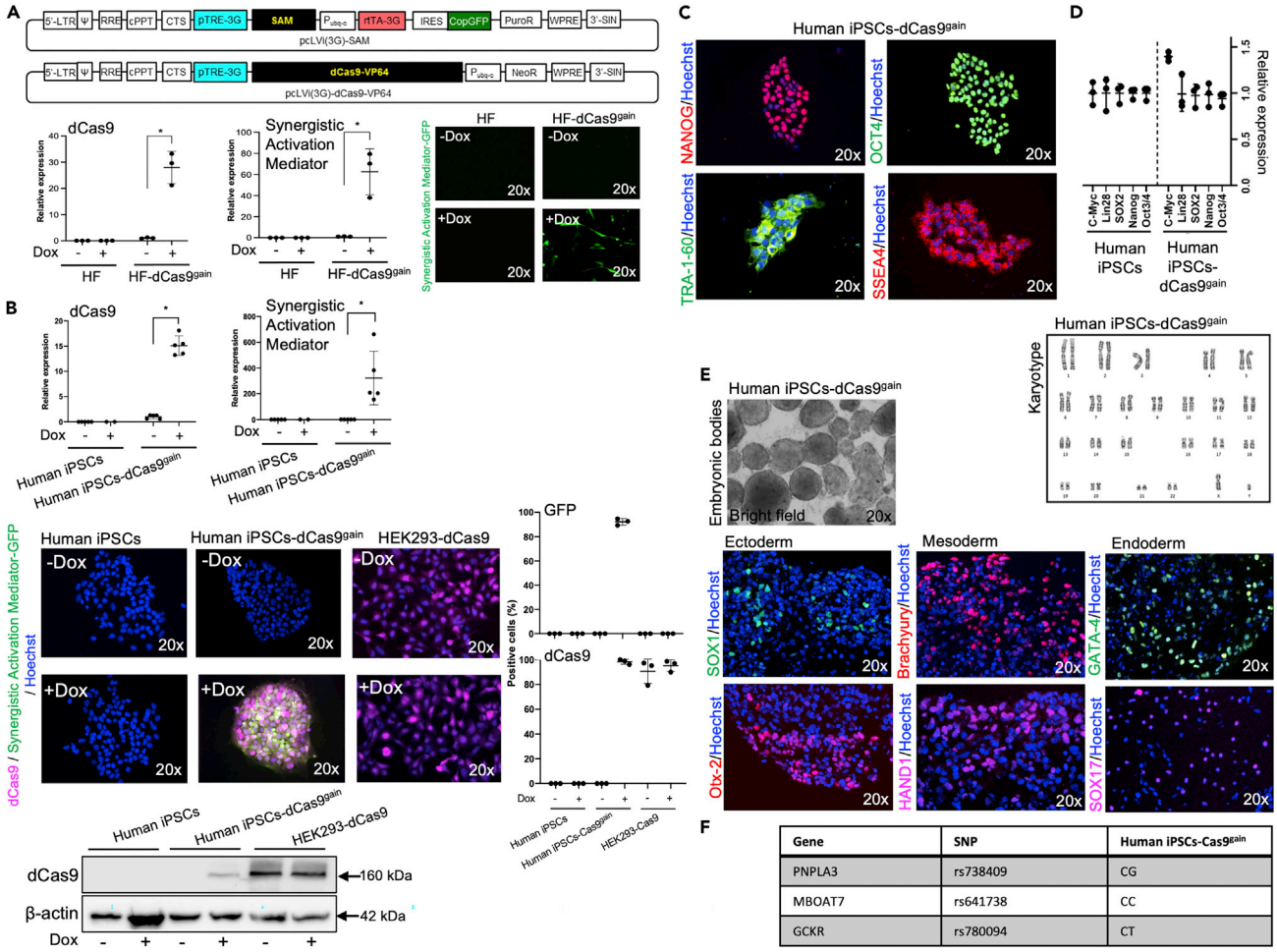

F

Gene	SNP	Human iPSCs-Cas9gain
PNPLA3	rs738409	CG
MBOAT7	rs641738	CC
GCKR	rs780094	CT

Figure 1. Generation of custom-engineered hiPSCs-dCas9^{gain}

(A) Schematic diagram of the lentiviral vectors: pcLVi(3G)-SAM containing a TetOn system comprising of a tetracycline response element (pTRE-3g), a reverse tetracycline-controlled reverse transactivator (rtTA-3G), green fluorescent protein (GFP), a puromycin antibiotic selection cassette gene (PuroR), and the synergistic activation mediator (SAM). pcLVi(3G)-dCas9-VP64 containing a tetracycline response element (pTRE-3g), a neomycin antibiotic selection cassette gene (NeoR), and the deactivated CRISPR/Cas9 transcription activator VP64 (dCas9-VP64). Quantitative gene expression analysis of Cas9 and SAM normalized to ACTB in human fibroblasts transduced with lentiviral vector for dCas9-VP64 (HFs-dCas9^{gain}) and non-transduced HF as control in the presence or absence of DOX (*p = 0.0168, Welch's t-test). Quantitative gene expression analysis of SAM normalized to ACTB transduced with lentiviral vector for SAM in HFs or HFs-dCas9^{gain} (*p = 0.0394, Welch's t-test). In-live GFP-fluorescence of synergistic activation mediator in HFFs or HFFs-dCas9^{gain} with and without DOX treatment. Data are represented as mean ± SD

(B) Quantitative gene expression analysis of dCas9 and SAM normalized to ACTB in human iPSCs derived from fibroblasts transduced with lentiviral vector for dCas9-VP64 (Human iPSCs-dCas9^{gain}) and non-transduced human iPSCs as control in the presence or absence of DOX (*p < 0.0001, Welch's t-test). Quantitative gene expression analysis of SAM normalized to ACTB transduced with lentiviral vector for SAM in Human iPSCs or Human iPSCs-dCas9^{gain} (*p < 0.05, Welch's t-test). Immunofluorescence micrographs of dCas9 and GFP in Human iPSCs or Human iPSCs-dCas9^{gain} with and without DOX treatment; HEK239-dCas9 was used as control. Western blot analysis of dCas9 and β-actin in human iPSCs and human iPSCs-Cas9^{gain} in the presence or absence of DOX; HEK239-dCas9 was used as control. Also shown is the Quantification of GFP and Cas9 in human iPSCs, human iPSCs-Cas9gain, and HEK293-Cas9 in the presence or absence of DOX. Data are represented as mean ± SD

(C) Immunofluorescence micrographs of pluripotency markers Nanog, Oct4, TRA-1-60, and SSEA-4 in human iPSCs-Cas9^{gain}. Quantitative gene expression analysis of pluripotency markers c-myc, Lin28, Sox2, Nanog, and Oct3/4 normalized to ACTB of human iPSCs and human iPSCs-Cas9^{gain}.

(D) Human iPSCs-dCas9^{gain} carries normal male karyotype in G-banding analysis.

(E) Bright-field micrograph of human iPSCs-dCas9^{gain} forming embryonic bodies after 20 days in culture. Immunofluorescence micrographs of the three germ layer markers: Ectoderm (Otx-2; SOX1), Mesoderm (HAND1; Brachuyry), and Endoderm (SOX17; GATA-4).

(F) Genotyping results of human iPSCs-Cas9^{gain}: PNPLA3 (rs738409) CT-heterozygous, MBOAT7 (rs641738) CC-major homozygous, and GCKR (rs780094) CT-heterozygous.

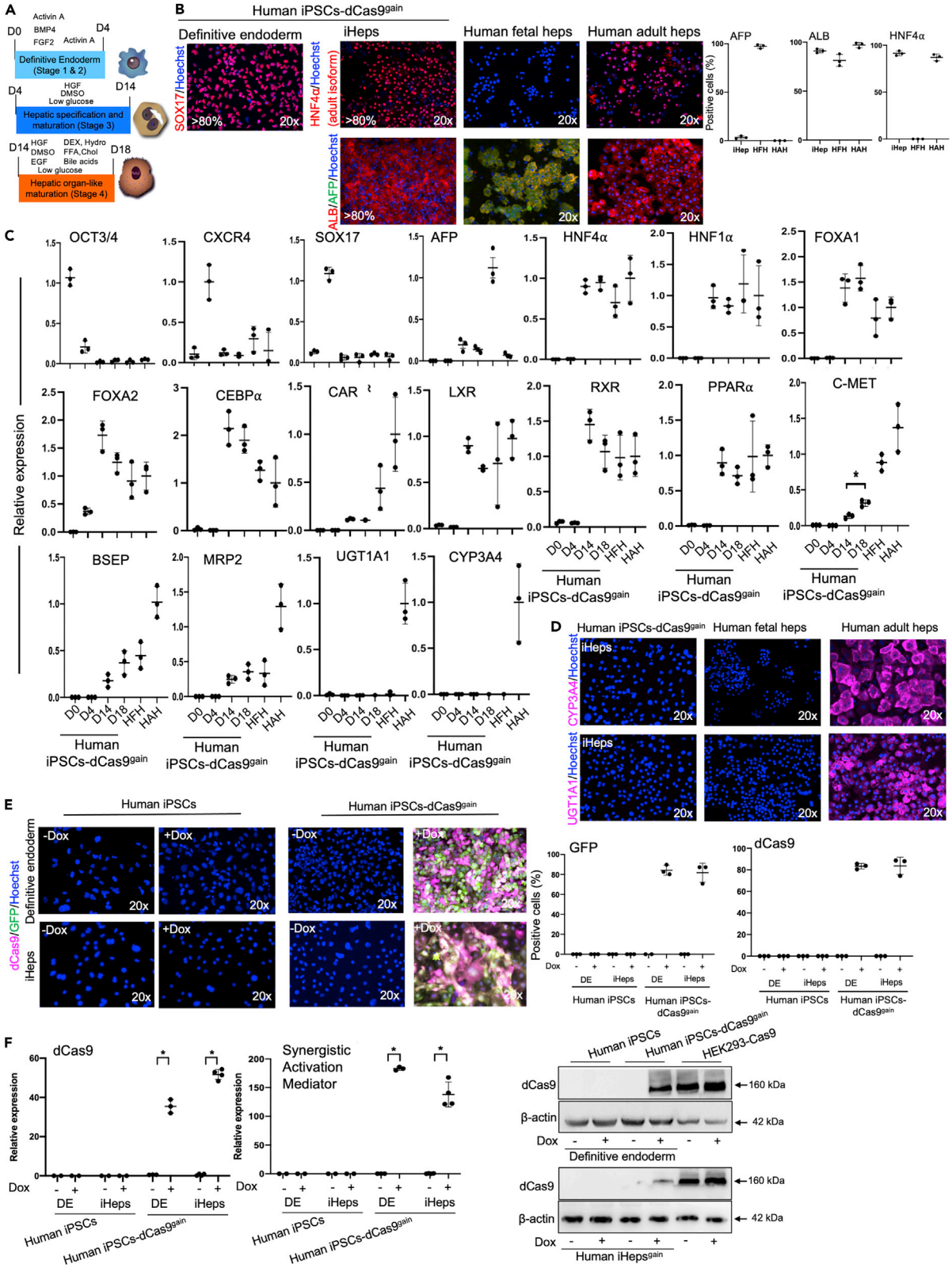
A
Activin A
D0
BMP4
FGF2
D4
Activin A
Definitive Endoderm (Stage 1 & 2)
D4
HGF
DMSO
Low glucose
D14
Hepatic specification and maturation (Stage 3)
D14
HGF
DMSO
EGF
DEX, Hydro
FFA,Chol
Bile acids
Low glucose
D18
Hepatic organ-like maturation (Stage 4)
B
Human iPSCs-dCas9gain
Definitive endoderm
iHeps
Human fetal heps
Human adult heps
SOX17/Hoechst
HNF4α/Hoechst (adult isoform)
ALB/AFP/Hoechst
>80%
20x
AFP
ALB
HNF4α
Positive cells (%)
iHep HFH HAH
C
OCT3/4
CXCR4
SOX17
AFP
HNF4α
HNF1α
FOXA1
FOXA2
CEBPα
CAR
LXR
RXR
PPARα
C-MET
BSEP
MRP2
UGT1A1
CYP3A4
Relative expression
D0 D4 D14 D18 HFH HAH
Human iPSCs-dCas9gain
D
Human iPSCs-dCas9gain
Human fetal heps
Human adult heps
CYP3A4/Hoechst
UGT1A1/Hoechst
iHeps
20x
E
Human iPSCs
Human iPSCs-dCas9gain
-Dox
+Dox
dCas9/GFP/Hoechst
Definitive endoderm
iHeps
20x
GFP
dCas9
Positive cells (%)
Dox
DE
iHeps
Human iPSCs
Human iPSCs-dCas9gain
F
dCas9
Synergistic Activation Mediator
Relative expression
Dox
DE
iHeps
Human iPSCs
Human iPSCs-dCas9gain
Human iPSCs
Human iPSCs-dCas9gain
HEK293-Cas9
dCas9
β-actin
160 kDa
42 kDa
Dox
Definitive endoderm
dCas9
β-actin
160 kDa
42 kDa
Dox
Human iHepsgain

Figure 2. Characterization of hepatocyte-derived custom-engineered hiPSCs-Cas9^{gain}

(A) Schematic illustration of hiPSC-dCas9^{gain} differentiation into hepatocytes like cells with the four main stages of differentiation by sequential addition of defined medium containing Activin A, BMP4, FGF2 (stage 1); Activin A (stage 2); dimethyl sulfoxide (DMSO), and hepatocyte growth factor (HGF) (stage 3); epidermal growth factor (EGF), dexamethasone (DEX), hydrocortisone (Hydro), free fatty acids (FFA), cholesterol (Chol), and bile acids (stage 4).

(B) Immunofluorescence micrographs of hiPSC-dCas9^{gain} for SOX17 show more than 80% of the cells positive for SOX17 after definitive endoderm induction stage 2. Immunofluorescence micrographs after hepatocyte differentiation stage 3 show protein expression of the adult isoform of HNF4a comparable to primary human hepatocytes (>80% respectively), expression of albumin comparable to primary human hepatocytes (>80% respectively), and no expression of α-fetoprotein (AFP); freshly isolated human fetal and adult hepatocytes were used as controls. Graphs showing quantification of cells expressing HNF4α, albumin, and alfa fetoprotein positive cells in iHep^{gain}, human fetal hepatocytes, and human adult hepatocytes.

(C) Quantitative gene expression analysis of undifferentiated hiPSC-dCas9^{gain} (D0), Definitive endoderm (DE) (D4), Stage 3 of the hepatic differentiation (D14), Stage 4 of the hepatic differentiation (D18). qPCR is shown for genes encoding octamer-binding transcription factor 3/4 (OCT3/4), C-X-C motif chemokine receptor 4 (CXCR4), SRY-box 17 (Sox17), hepatocyte nuclear factor-4-alpha (HNF4a), hepatocyte nuclear factor-1-alpha (HNF1a), forkhead box A1 (FOXA1), forkhead box A2 (FOXA2), CCAAT enhancer-binding protein alpha (CEBPa), constitutive androstane receptor (CAR), liver X receptor (LXR), retinoid X receptor (RXR), peroxisome proliferator-activated receptor alpha (PPARa), Met, ATP binding cassette subfamily B member 11 (BSEP), ATP binding cassette subfamily C member 2 (MRP2), alpha-fetoprotein (AFP), UDP glucuronyltransferase family 1 member A1 (UGT1A1) and cytochrome P450 family 3 subfamily A member 4 (CYP3A4). Human adult hepatocytes and human fetal hepatocytes were included as controls. Data are represented as mean ± SD

(D) Immunofluorescence micrographs of hiPSC-dCas9^{gain} at stage 3 of hepatic differentiation (D14) stained for CYP3A4 and UGT1A1 compared to primary human adult and fetal hepatocytes.

(E) Immunofluorescence micrographs for GFP and dCas9 of control human iPSCs and human iPSCs-Cas9^{gain} the end of stage 2 (DE) and stage 3 (iHep) in the presence or absence of DOX. Quantification of GFP and Cas9 in human iPSCs and human iPSCs-Cas9^{gain} at the end of stage 2 (DE) and stage 3 (iHep) in the presence or absence of DOX.

(F) Quantitative gene expression analysis of dCas9 and synergistic activation mediator (SAM) normalized to ACTB at in hiPSCs and hiPSC-dCas9^{gain} at different stages of hepatic differentiation: Definitive endoderm (DE), Stage 3 (iHeps) in the presence or absence of DOX (*$p < 0.05$, Welch's t test). Western Blot analysis of dCas9 in hiPSC and hiPSC-dCas9^{gain} in the presence or absence of DOX at definitive endoderm (Stage 2) and in human iHeps^{gain} (Stage 3). HEK-dCas9 was used as control.

isoform of hepatocyte nuclear factor 4 alpha (HNF4α), (Figure 2B). On day 14 of differentiation (stage 3), more than 80% of human iPSCs-dCas9^{gain}-derived hepatocytes (human iHeps^{gain}) expressed the adult isoform of HNF4α and albumin, and human iHeps^{gain} did not express the hepatocyte immature marker alpha-fetoprotein (AFP) (Figures 2B and S2). Analysis of mRNA expression at the end of stage 3 and 4 of differentiation showed upregulation of liver-enriched transcription factors such as HNF4α, hepatocyte nuclear factor 1 (HNF1α), forkhead box protein A1 (FOXA1), forkhead box protein A2 (FOXA2), CCAAT/enhancer-binding protein 1 alpha (CEBPα), constitutive androstane receptor (CAR), liver X receptor (LXR), retinoid X receptor (RXR), and peroxisome proliferator-activated receptor (PPARα) to levels approximating those for human primary hepatocytes (Figure 2C). However, we did not detect expression of Cytochrome P450 3A4 (CYP3A4) or glucuronosyltransferase 1 family, polypeptide A1 (UGT1A1), as assessed by mRNA and protein expression (Figures 2C and 2D). To test if hepatocyte-directed differentiation could be enhanced by programmable expression of Cas9 and the gene activator (SAM), protein and mRNA expression of these two genes were assessed at the different stages of differentiation. Cells at the definitive endoderm stage and iHeps derived from human iPSCs-dCas9^{gain} showed highly inducible dCas9 and SAM-GFP expression and function after Dox exposure (Figures 2E, 2F, and S3).

Programmable activation of hepatocyte-specific genes in Heps^{gain} using guide RNAs

Since expression levels of CYP3A4 and UGT1A1 were not detected following the final maturation step of hepatocyte-directed differentiation, these genes were selected to test the efficiency of our gene programmable system in human iHeps^{gain}. To induce these clinically relevant metabolic genes, iHeps^{gain} were transduced with lentiviral vectors coding gRNAs for CYP3A4 and UGT1A1, with >90% transduction efficiency (Figure S4A). We designed two guide RNAs for transcriptional activation of CYP3A4 to bind in the promoter region of CYP3A4 on Chromosome 7 and three guide RNAs for the transcriptional activation of UGT1A1 were also designed to bind in the promoter region of UGT1A1 on Chromosome 2. Only specific guide RNAs with no predicted off-target effects were screened and selected. gRNAs were packed in a lentiviral vector for transduction containing the fluorescent protein (RFP) for transduction identification purposes. Both genes were successfully and significantly induced and activated, as assessed by mRNA and protein expression, in the iHeps^{gain} by the gRNAs under Dox exposure, and were expressed at levels comparable to that found in adult primary human hepatocytes (Figures 3A and S5). mRNA expression of CYP3A4 and UGT1A1 were 44% and 61%, respectively, compared to that of adult human hepatocytes and no significant difference was observed in mRNA expression when iHeps^{gain} were compared to human adult hepatocytes. The average CYP3A4 protein expression was 93% of that observed in adult human hepatocytes and UGT1A1 protein expression was significantly induced in DOX-exposed human iHeps^{gain} representing 25% of that observed in adult human hepatocytes (Figure 3A).

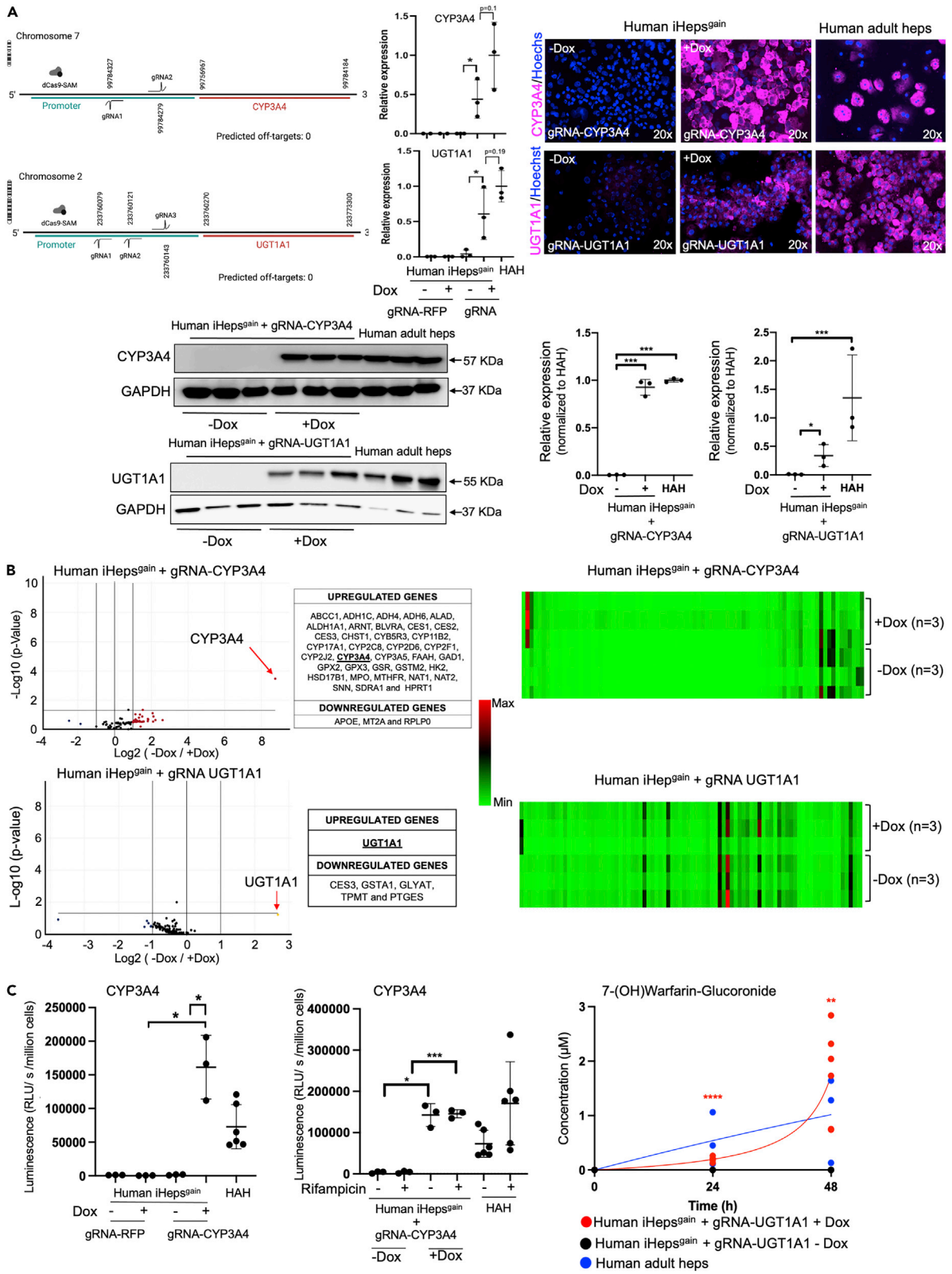
A
Chromosome 7
dCas9-SAM
Promoter
gRNA1
gRNA2
CYP3A4
Predicted off-targets: 0
Chromosome 2
gRNA3
UGT1A1
Predicted off-targets: 0
CYP3A4
UGT1A1
Relative expression
Human iHepsgain HAH
Dox
gRNA-RFP
gRNA
Human iHepsgain
Human adult heps
CYP3A4/Hoechs
UGT1A1/Hoechst
-Dox
+Dox
gRNA-CYP3A4
gRNA-UGT1A1
20x
Human iHepsgain + gRNA-CYP3A4
Human adult heps
CYP3A4
GAPDH
57 KDa
37 KDa
-Dox
+Dox
Human iHepsgain + gRNA-UGT1A1
UGT1A1
55 KDa
Relative expression (normalized to HAH)
Human iHepsgain + gRNA-CYP3A4
Human iHepsgain + gRNA-UGT1A1
B
Human iHepsgain + gRNA-CYP3A4
-Log10 (p-Value)
Log2 (-Dox / +Dox)
UPREGULATED GENES
ABCC1, ADH1C, ADH4, ADH6, ALAD, ALDH1A1, ARNT, BLVRA, CES1, CES2, CES3, CHST1, CYB5R3, CYP11B2, CYP17A1, CYP2C8, CYP2D6, CYP2F1, CYP2J2, CYP3A4, CYP3A5, FAAH, GAD1, GPX2, GPX3, GSR, GSTM2, HK2, HSD17B1, MPO, MTHFR, NAT1, NAT2, SNN, SDRA1 and HPRT1
DOWNREGULATED GENES
APOE, MT2A and RPLP0
Human iHepsgain + gRNA-CYP3A4
+Dox (n=3)
-Dox (n=3)
Max
Min
Human iHepgain + gRNA UGT1A1
L-og10 (p-value)
UPREGULATED GENES
UGT1A1
DOWNREGULATED GENES
CES3, GSTA1, GLYAT, TPMT and PTGES
Human iHepgain + gRNA UGT1A1
C
CYP3A4
Luminescence (RLU/ s /million cells)
Human iHepsgain HAH
Dox
gRNA-RFP
gRNA-CYP3A4
Rifampicin
-Dox
+Dox
7-(OH)Warfarin-Glucoronide
Concentration (μM)
Time (h)
Human iHepsgain + gRNA-UGT1A1 + Dox
Human iHepsgain + gRNA-UGT1A1 - Dox
Human adult heps

Figure 3. Transcriptional activation of CYP3A4 and UGT1A1 in Custom-Engineered human iHep-dCas9^{gain}

(A) Schematic illustration of the gRNA binding site in the promoter region of CYP3A4 and UGT1A1 gene. No off-targets were predictable. Quantitative gene expression analysis of CYP3A4 and UGT1A1 in iHep-dCas9^{gain} transduced with scrambled gRNA and gRNA-RFP or gRNA-CYP3A4 or gRNA-UGT1A1 in the presence and absence of DOX normalized to ACTB (*p < 0.05, Welch's t-test). Human adult hepatocytes (HAH) were used as control. Immunofluorescence micrographs CYP3A4 and UGT1A1 in iHep-dCas9^{gain} under the presence or absence of DOX transduced with gRNA-CYP3A4 or gRNA-UGT1A1. Freshly isolated human hepatocytes were used as control. Western Blot analysis and quantification: on the left the relative expression of CYP3A4 (CYP3A4; ***p < 0.0001, Ordinary one-way ANOVA with Turkey's multiple comparisons) and UGT1A1 (UGT1A1; *p = 0.0427, unpaired t-test) in iHep-dCas9gain transduced with gRNA-CYP3A4 or UGT1A1 under the presence or absence of DOX. On the right, the expression of CYP3A4 and UGT1A1 in iHep-dCas9gain transduced with gRNA-CYP3A4 or UGT1A1 under the presence or absence of DOX normalized to human adult hepatocyte. The relative expression average of human adult hepatocytes was set up as 1. Data are represented as mean ± SD

(B) Volcano plot and heatmap showing differential gene expression of iHep-dCas9^{gain} transduced with gRNA-CYP3A4 under the presence or absence of DOX. Volcano plot and heatmap showing differential gene expression of iHep-dCas9gain transduced with gRNA-UGT1A1 under the presence or absence of DOX.

(C) CYP3A4 activity of iHep-dCas9^{gain} transduced with a scrambled gRNA and RFP or gRNA CYP3A4 in the presence or absence of DOX (*p < 0.05, Welch's t-test) and Rifampicin (*p = 0.01, ***p = 0.0008, Welch's t-test). UGT1A1 activity assessed by 7(OH)Warfarin-Glucuronide production over time in iHep-dCas9^{gain} transduced with gRNA-UGT1A1 in the presence or absence of DOX (****p < 0.0001, **p = 0.0041, Welch's t-test). Adult human hepatocytes were used as control. Data are represented as mean ± SD.

No significant protein expression difference was identified when comparing iHeps^{gain} and freshly isolated human adult hepatocytes (CYP3A4 p = 0.2364; UGT1A1 p = 0.0730).

To assess the selectivity of gene activation, we analyzed the transcriptomic signature of the iHeps^{gain} after CYP3A4 or UGT1A1 gRNA exposure. Only either CYP3A4 or UGT1A1 was significantly and selectively induced respectively (Figure 3B). Interestingly, the activation of CYP3A4 or UGT1A1 by gRNAs induced minimal upregulation or downregulation of other genes related to drug metabolism (Figure 3B), indicating the absence of off-target effect on other metabolic genes (Table S3 and Figure S4).

To understand if gene activation by gRNAs in iHeps^{gain} would result in post-translational activation and enzymatic function, we performed the P450-Glo assay for CYP3A4 activity by quantification of luciferin production converted from proluciferin substrate[25] and performed quantification of 7-(OH) Warfarin-Glucuronide glucuronidated from 7-(OH) warfarin by UGT1A1 using the high-performance liquid chromatography assay.[26] Human iHeps^{gain} under Dox exposure and programmed selected gRNAs exhibited CYP3A4 or UGT1A1 activities comparable or even higher than those observed in freshly isolated adult human hepatocytes (Figure 3C). We confirmed that Dox exposure did not affect CYP3A4 or UGT1A1 expression in freshly isolated human adult hepatocytes (Figure S6A). Moreover, gene activation by gRNAs using viral vectors did not induce apoptotic pathways such as caspase-3 (Figure S7A). However, rifampicin-driven CYP3A4 activity inducibility was limited in iHeps^{gain} (Figures 3C and S8).

Biofabrication of synthetic human liver tissue with programmable gene activation

After generating hepatocytes from human iPSCs-dCas9^{gain}, we determined that generating human liver tissue would require reproducing other elements of the liver microenvironment.[9,27,28] Therefore, to biofabricate synthetic human liver tissue, human iHeps^{gain}, human vascular endothelial cells, human fibroblasts, and human mesenchymal stem cells were populated onto 3D-printed constructs (Figures 4A and 4B). Although hepatocytes constitute most of the parenchymal space, supportive non-parenchymal cells (mesenchymal stromal cells, endothelial cells, and fibroblasts) enhance structural polarity and cellular stability.[27,29–31] iHeps^{gain} (representing 85% of the cellular mass), human vascular endothelial cells (representing 10% of the cellular mass), human mesenchymal stem cells (hMSCs, representing 2.5% of the cellular mass), and human fibroblasts (representing 2.5% of the cellular mass) were seeded onto a 3D-printed construct based on the cellular content of a liver lobe.[32] Expression of CD31 for human endothelial cells, CD44 for human mesenchymal stem cells, and αSMA for human fibroblast was confirmed in the synthetic human liver^{gain} tissue (Figure 4B). iHeps^{gain} showed inducible SAM-GFP expression under Dox exposure while both iHeps^{gain} (-Dox and +Dox) showed similar expression of RFP/gRNAs transduction (>90%) in the synthetic human liver^{gain} tissues well (Figures 4C and S4A). Moreover, synthetic human liver^{gain} expressed dCas9, CYP3A4, and UGT1A1 protein diffusely (Figures 4D and 4E). By applying a different format of 3D-multicellular approach, we corroborated CYP3A4 activity under Dox exposure and critical markers of cell-cell and cell-extracellular matrix contacts such as ZO-1 and ITGB1 were significantly improved when compared to 2D cell culture format (Figures 4D, S9, and S10), indicating that the biofabricated 3D synthetic human liver^{gain} tissue was functionally programmable and expressed critical cellular communication molecules to a high degree.

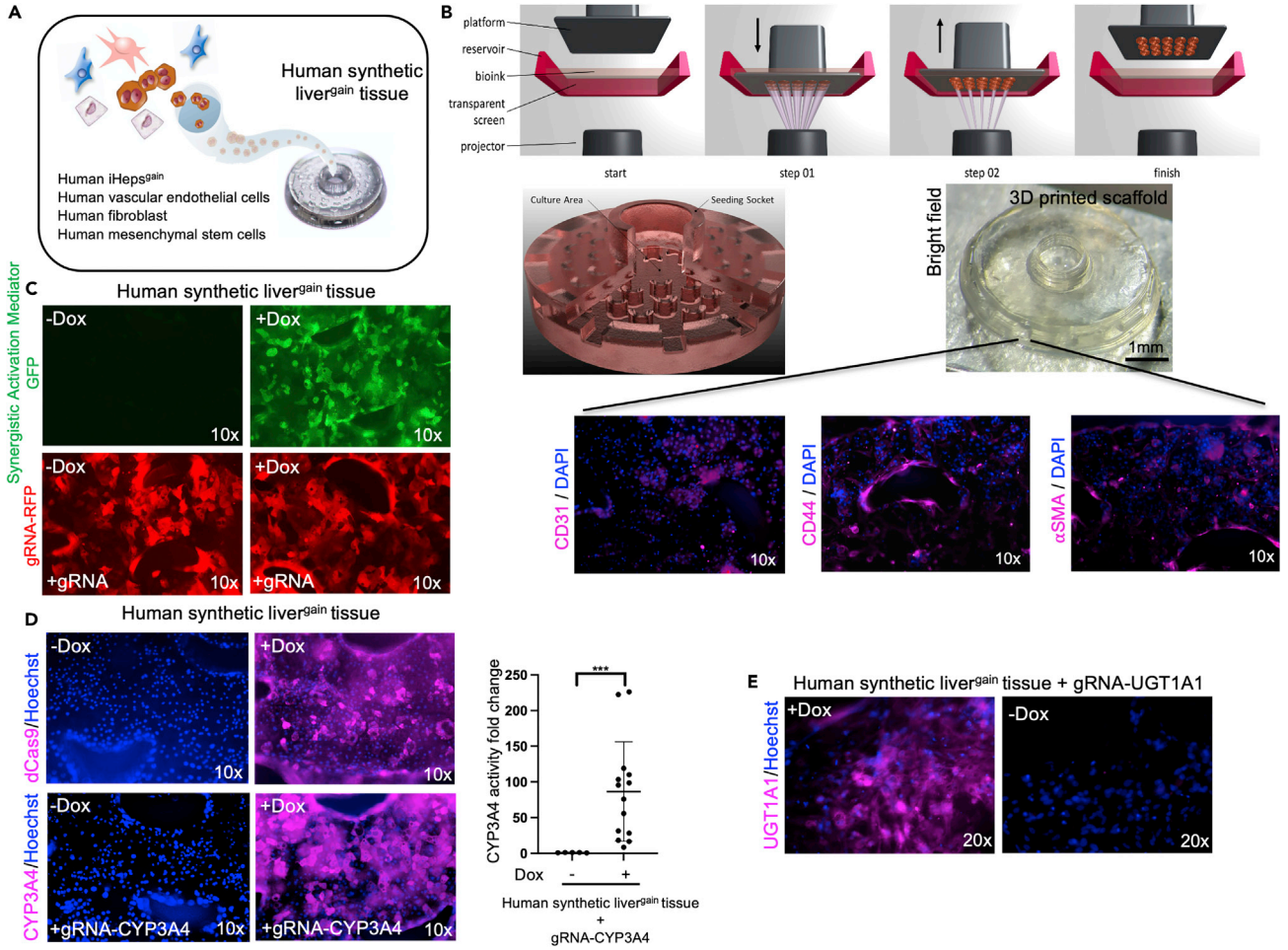

Figure 4. Bioengineering of hiPSC-derived dCas9^{gain} tissue expressing CYP3A4 and UGT1A1

(A) Schematic representation of the cell types involved in the seeding process: Human iHep^{gain}, human vascular endothelial cells, human fibroblasts, and human mesenchymal stem cells.

(B) Schematic representation of Haemobrick production via a stereolithographic bioprinting process. The platform is submerged into a photosensitive bioink leaving a gap of defined layer thickness between itself and the transparent screen. A photomask is projected through the transparent screen onto the platform curing the bioink to a hydrogel layer (step 01). The size of the gap increases by raising the platform. The photomask of the next layer is projected onto the previous one accordingly (step 02). This process is repeated stacking hydrogel layers onto each other until the complete object has been created sequentially. Cells can be cultured in the culture area after application through the seeding socket. Immunofluorescence micrograph of human synthetic livergain tissue showing the human vascular endothelial cells (CD31 positive cells), human mesenchymal stem cells (CD44 positive cells), and human fibroblast (αSMA positive cells).

(C) Immunofluorescence micrographs of human synthetic liver^{gain} tissue showing expression of GFP (Synergistic Activation Mediator) in the presence or absence of DOX. Moreover, also shown are Immunofluorescence micrographs of human synthetic liver^{gain} tissue showing expression of red fluorescent protein (RFP) demonstrating that high transduction of lentivirus containing gRNAs was achieved in human synthetic liver^{gain} tissue exposed to DOX and in the control group non-DOX treated.

(D) Immunofluorescence micrographs of human synthetic liver^{gain} tissue for dCas9 and CYP3A4 transduced with gRNA-CYP3A4 in the presence or absence of DOX. CYP3A4 activity of human synthetic liver^{gain} tissue transduced with gRNA-CYP3A4 in the presence or absence of DOX (***$p < 0.0005$, Welch's-test). Data are represented as mean ± SD.

(E) Immunofluorescence micrographs of human synthetic liver^{gain} tissue for UGT1A1 transduced with gRNA-UGT1A1 in the presence or absence of DOX.

DISCUSSION

Generating human liver tissue that incorporates elements from synthetic biology that allows augmentation of the cell's genetic programs to change the tissue functional capabilities and behavior would not only provide an alternative strategy for the treatment of patients with terminal liver failure but also represent a powerful method to study genomic scale gain-of-function approaches to uncover biological mechanisms, as well as to enhance drug discovery/development. In this study, we demonstrated that human liver tissue

generated from human iPSCs genetically modified to express an inducible dCas9-based gene activation system is responsive and programmable to express mature and clinically relevant genes CYP3A4 and UGT1A1 under control of guide RNA delivery, thus, inducing post-translational activation and functions comparable to freshly isolated human primary hepatocytes.

By engineering human-induced pluripotent cells carrying an inducible dCas9-based activation system or CRISPRa, programmed guide gene expression exhibited a high degree of consistency, with nearly all resulting cells effectively targeted by guide RNAs. This is an important consideration when consistent and adult-level gene expression is desirable across a large population of cells and tissues.[14] The guide RNA delivery method can be selected depending on the desired gene, timeline, and specificity of the study. In the present study and as a proof-of-principle, we use a lentiviral vector to guarantee high transduction efficiency in human cells. However, other delivery methods could be used efficiently such as lipid nanoparticles,[33] adeno associate viruses,[34] or fusion proteins.[35]

Moreover, human-induced pluripotent cells are generated by forced expression of specific pluripotency transcription factors[36] and they have the ability to proliferate infinitely and differentiate into cells of all three germ layers,[37] and although a great deal of progress has been made investigating not only hepatocyte differentiation capacity of iPSCs but other cell types of the liver,[9] cells that replicate the ability of human primary adult hepatocytes to metabolize drugs *in vitro*, regenerate livers, or to have advanced functions on demand has not been achieved. First, this human iPSC-CRISPRa-based system provides the advantage of upregulating endogenous genes that can be studied in both healthy and diseased genetic backgrounds (e.g. mutations in introns or exons),[38,39] which could be a very valuable tool for drug discovery and preclinical programs. Second, the system goes beyond drug discovery or basic biology and could represent a reliable source for future liver bioengineering approaches that can be adapted to other organ systems. Clinical application of bioengineered liver tissue or grafts will require the generation of high numbers of iPS-Heps with functionality equal to that of primary human hepatocytes. As a proof-of-principle, we programmed the expression and function of two mature, clinically relevant liver-specific enzymes CYP3A4 and UGT1A1 which were not fully expressed using our conventional hepatocyte-directed differentiation protocol[15] (Figure 2). Using this inducible dCas9-based activation system strategy, we were able to maintain the expression of hepatocyte-enriched transcription factors important for hepatocyte function, to induce expression of the clinically relevant enzymes CYP3A4 and UGT1A1, and most importantly to demonstrate metabolic activity at equal levels or higher than those observed in freshly isolated primary human adult hepatocytes. These human iPSCs-dCas9^{gain} could be used to generate any cell type or tissue and programmed expression of one or many genes. Thus, the current approach represents a powerful tool that can be used to investigate signaling pathways and to generate human disease models as well. Furthermore, applications of human iPSCs-dCas9^{gain} in positive and negative selection screens will enable the analysis of many kinds of genetic components, varying from protein-coding genes or non-coding RNA elements to even epigenetic modifiers in diverse biological processes.

Future programming of engineered human iPSCs carrying the dCas9 complex can further expand the dCas9 toolbox. Additional developments of the dCas9-based gene activation system may include improvement of features such as customizability of the gRNA scaffold sequence composition and stability[14] or improvements in the potency of a new generation of gene activation systems such as the catalytic domain of the histone acetyltransferase CBP[40] or SPH which combines components of SAM and other activators.[41] An important concern for any dCas9-based technology is the specificity of the desired effect. It has been demonstrated that dCas9 binds promiscuously throughout the genome[42] causing potential off-target effects which is a critical concern for the preclinical and clinical application of the dCas9-based gene activation system and the engineered cell therapies. However, several encouraging strategies have been developed to mitigate any potential off-target responses, such as the sgRNA design optimization using computational methods, transcriptome analysis, and functional screening after dCas9 treatment. A recent CRISPR/Cas9 clinical application has demonstrated the safety of the system with no evidence of off-target editing in at least two patients.[43]

Importantly, using custom-engineered human iPSCs and multicellular systems, human synthetic liver tissue was biofabricated that was able to be genetically programmed. While entire genetic programs that control the more than 500 hepatocyte functions represent a complex system and many genes and susceptibilities play important roles, this study was limited to the modification of only two clinically relevant genes. Future

human synthetic liver tissue prototypes should incorporate a greater number of programmable gene induction simultaneously by utilizing multiple gRNAs against many genes. Moreover, while the biofabricated human synthetic liver tissue was able to demonstrate cytochrome activity at the level of freshly isolated human hepatocytes, we were not able to document comparable inducibility after exposure to rifampicin (a prototypical CYP3A4 inducer). The lack of expression and function of other gene programs related to the capacity of cytochrome inducibility might be the major reason responsible for this failure. However, systems such as human iPSCs-Cas9^{gain} can be used to interrogate metabolic inducibility and maturation by screening activators or co-activators of functional enzymes to design improved hepatic differentiation protocols so that hepatocytes express CYP3A4 and UGT1A1 naturally. In the current 3D cell culture formats, we observed increase in cell-cell and cell-matrix proteins, when compared to 2D cultures. However, the 3D spheroid multicellular system did not show additive effect on the gene functions targeted by the Dox-mediated gene activation (dCas9-SAM system) such CYP3A4 activity. Future experiments will explore the incorporation of other organotypic cell culture formats and the use of animal models or liver repopulation and regeneration to decipher critical gene circuits and programs.

Synthetic biology is poised to improve gene- and engineered-cell-based treatments for many diseases by providing precise control over the intensity, timing, and context of therapeutic intervention. The proof of principle experiments presented here used human iPSCs with controllable expression of the CRISPR-Cas9 guide RNA-directed synergistic activation mediator (SAM) which is capable of transcriptionally activating target endogenous genes to generate human liver tissue with advanced programmable functions. This strategy could be adapted to interrogate other pathways, molecules, cell types, and diseases. Future studies will optimize these tools for disease modeling within structured microphysiology systems (MPS) and organoid-MPS, including critical diseases impacting the liver.[39] These studies outline a strategy for custom-engineering liver tissue for future biological, drug discovery/development, and potential clinical applications.

Limitations of the study

The present study demonstrated that synthetic human liver tissue with modifiable functional genetic programs can be generated. Importantly, using human iPSCs with target gene expression controlled by a guide RNA-directed CRISPR-Cas9 synergistic activation mediator (SAM), the fabricated synthetic human liver tissues is capable of transcriptionally activating target endogenous genes such as CYP3A4 and UGT1A1. While we demonstrated activity of both CYP3A4 and UGT1A1 proteins, this study was limited to the modification of only these two genes. Future human liver tissue prototypes should incorporate a greater number of entire pathways by incorporating several genes and transcriptional factors as gRNA-mini libraries. Moreover, while the biofabricated human synthetic human liver tissue was used to activate targeted endogenous genes, this study did not test the knockdown or knockout of genes. Thus, future developments will incorporate the generation of human iPSCs with CRISPR-Cas9-based toolbox to perform any type of gene regulation. Our study also had limitations in the generation of only one liver cell type—hepatocyte—and in the full hepatic metabolic profiling due to the non-fully mature hepatocytes produced from human iPSCs.

STAR★METHODS

Detailed methods are provided in the online version of this paper and include the following:

- KEY RESOURCES TABLE
- RESOURCE AVAILABILITY
  - Lead contact
  - Material availability
  - Data and code availability
- EXPERIMENTAL MODEL AND SUBJECT DETAILS
  - Primary human fetal and adult hepatocytes
- METHOD DETAILS
  - Production of high titer lentivirus
  - Lentiviral transduction of human fetal fibroblasts
  - Generation and culture of human iPSC lines
  - Embryoid body formation
  - Cell culture

- Differentiation of human iPSCs into hepatocytes (iHep^{gain})
- dCas9^{gain} activation and gRNA delivery in the iHep^{gain}
- Quantitative real-time PCR
- Western blot
- Immunofluorescence
- Transcription profiling by RT^2 profiler PCR array
- CPY3A4 functional analysis
- UGT1A1 functional analysis
- Human synthetic liver^{gain} tissue

● QUANTIFICATION AND STATISTICAL ANALYSIS

SUPPLEMENTAL INFORMATION

Supplemental information can be found online at https://doi.org/10.1016/j.isci.2022.105503.

ACKNOWLEDGMENTS

This work was supported by NIH grants DK099257 and TR003289 to A.S.-G., DK096990 to I.J.F. and A.S.-G, DK117881, DK119973, TR002383 to D.L.T., and A.S.-G. This work was also supported by NIH grant 1P30DK120531-01 to the Human Synthetic Liver Biology Core (A.S.-G.) and the Pittsburgh Liver Research Center (PLRC).

AUTHOR CONTRIBUTIONS

A.S.-G., conceived and designed the study; K.M., R.M.F., N.H., T.M., R.D.-A., L.A.P.F., A.C.-H., Z.C., and L.V., performed data acquisition; R.M.F., N.H., K.M., C.F., T.M., R.D.-A., L.A.P.F., A.C.-H., L.V., K.T., and A.S.-G., analyzed and interpreted data; R.M.F., N.H., K.M., C.F., A.C.-H., I.J.F., and A.S.-G., established the human iPS cell lines used in this report and performed hepatic differentiation; assembly and characterization; K.M., R.M.F., N.H., L.V., D.L.T., and A.S.-G., analyzed functional and metabolic data; A.K.A., A.T., T.L., and L.K., designed and 3D-printed liver scaffolds; R.M.F., N.H., and A.S.-G., wrote the manuscript; K.M., R.M.F., N.H., T.M., R.D.-A., L.A.P.F., A.C.-H., L.V., A.K.A., A.T., T.L., L.K., K.T., D.L.T., I.J.F., and A.S.-G., participated in critical revision of the manuscript for intellectual content; A.S.-G., obtained funding. All authors contributed to the preparation of the manuscript.

DECLARATION OF INTERESTS

A.C.-H., K.T., I.J.F., and A.S.-G. are inventors on a provisional international patent application that describes hepatic differentiation of human pluripotent stem cells and liver repopulation (PCT/US2018/018032) and a provisional international patent application that describes the use of human-induced pluripotent stem cells for highly genetic engineering (PCT/US2017/044719). A.S.-G., J.G.-L., A.C.-H., and I.J.F. are co-founders and have a financial interest in Von Baer Wolff, Inc. a company focused on biofabrication of autologous human hepatocytes from stem cells technology. I.J.F. and A.S.-G. are co-founders and have a financial interest in Pittsburgh ReLiver Inc, a company focused on programming liver failure and their interests are managed by the Conflict-of-Interest Office at the University of Pittsburgh in accordance with their policies.

INCLUSION AND DIVERSITY

One or more of the authors of this paper self-identifies as an underrepresented ethnic minority in science.

Received: October 21, 2021
Revised: February 1, 2022
Accepted: November 1, 2022
Published: December 22, 2022

REFERENCES

1. Habka, D., Mann, D., Landes, R., and Soto-Gutierrez, A. (2015). Future economics of liver transplantation: a 20-year cost modeling forecast and the prospect of bioengineering autologous liver grafts. PLoS One *10*, e0131764. https://doi.org/10.1371/journal.pone.0131764.

2. Kwong, A.J., Kim, W.R., Lake, J.R., Smith, J.M., Schladt, D.P., Skeans, M.A., Noreen, S.M., Foutz, J., Booker, S.E., Cafarella, M., et al. (2021). OPTN/SRTR 2019 annual data report: liver. Am. J. Transplant. *21*, 208–315. https://doi.org/10.1111/ajt.16494.

3. Haep, N., Florentino, R.M., Squires, J.E., Bell, A., and Soto-Gutierrez, A. (2021). The inside-out of end-stage liver disease: hepatocytes are the keystone. Semin. Liver Dis. *41*, 213–224. https://doi.org/10.1055/s-0041-1725023.

4. Hartog, H., Hann, A., and Perera, M.T.P.R. (2022). Primary non-function of the liver allograft. Transplantation *106*, 117–128. https://doi.org/10.1097/TP.0000000000003682.

5. Ammori, J.B., Pelletier, S.J., Lynch, R., Cohn, J., Ads, Y., Campbell, D.A., and Englesbe, M.J. (2008). Incremental costs of post-liver transplantation complications. J. Am. Coll. Surg. *206*, 89–95. https://doi.org/10.1016/j.jamcollsurg.2007.06.292.

6. Eshmuminov, D., Becker, D., Bautista Borrego, L., Hefti, M., Schuler, M.J., Hagedorn, C., Muller, X., Mueller, M., Onder, C., Graf, R., et al. (2020). An integrated perfusion machine preserves injured human livers for 1 week. Nat. Biotechnol. *38*, 189–198. https://doi.org/10.1038/s41587-019-0374-x.

7. Li, X., and Burlak, C. (2020). Xenotransplantation literature update. Xenotransplantation *27*, e12607. https://doi.org/10.1111/xen.12607.

8. Rammohan, A., Reddy, M.S., Narasimhan, G., Rajalingam, R., Kaliamoorthy, I., Shanmugam, N., and Rela, M. (2019). Auxiliary partial orthotopic liver transplantation for selected noncirrhotic metabolic liver disease. Liver Transplant. *25*, 111–118. https://doi.org/10.1002/lt.25352.

9. Takeishi, K., Collin de l'Hortet, A., Wang, Y., Handa, K., Guzman-Lepe, J., Matsubara, K., Morita, K., Jang, S., Haep, N., Florentino, R.M., et al. (2020). Assembly and function of a bioengineered human liver for transplantation generated solely from induced pluripotent stem cells. Cell Rep. *31*, 107711. https://doi.org/10.1016/j.celrep.2020.107711.

10. Konermann, S., Brigham, M.D., Trevino, A.E., Joung, J., Abudayyeh, O.O., Barcena, C., Hsu, P.D., Habib, N., Gootenberg, J.S., Nishimasu, H., et al. (2015). Genome-scale transcriptional activation by an engineered CRISPR-Cas9 complex. Nature *517*, 583–588. https://doi.org/10.1038/nature14136.

11. Cong, L., Ran, F.A., Cox, D., Lin, S., Barretto, R., Habib, N., Hsu, P.D., Wu, X., Jiang, W., Marraffini, L.A., and Zhang, F. (2013). Multiplex genome engineering using CRISPR/Cas systems. Science *339*, 819–823. https://doi.org/10.1126/science.1231143.

12. Mali, P., Yang, L., Esvelt, K.M., Aach, J., Guell, M., DiCarlo, J.E., Norville, J.E., and Church, G.M. (2013). RNA-guided human genome engineering via Cas9. Science *339*, 823–826. https://doi.org/10.1126/science.1232033.

13. Qi, L.S., Larson, M.H., Gilbert, L.A., Doudna, J.A., Weissman, J.S., Arkin, A.P., and Lim, W.A. (2013). Repurposing CRISPR as an RNA-guided platform for sequence-specific control of gene expression. Cell *152*, 1173–1183. https://doi.org/10.1016/j.cell.2013.02.022.

14. Chavez, A., Tuttle, M., Pruitt, B.W., Ewen-Campen, B., Chari, R., Ter-Ovanesyan, D., Haque, S.J., Cecchi, R.J., Kowal, E.J.K., Buchthal, J., et al. (2016). Comparison of Cas9 activators in multiple species. Nat. Methods *13*, 563–567. https://doi.org/10.1038/nmeth.3871.

15. Collin de l'Hortet, A., Takeishi, K., Guzman-Lepe, J., Morita, K., Achreja, A., Popovic, B., Wang, Y., Handa, K., Mittal, A., Meurs, N., et al. (2019). Generation of human fatty livers using custom-engineered induced pluripotent stem cells with modifiable SIRT1 metabolism. Cell Metab. *30*, 385–401.e9. https://doi.org/10.1016/j.cmet.2019.06.017.

16. Platt, R.J., Chen, S., Zhou, Y., Yim, M.J., Swiech, L., Kempton, H.R., Dahlman, J.E., Parnas, O., Eisenhaure, T.M., Jovanovic, M., et al. (2014). CRISPR-Cas9 knockin mice for genome editing and cancer modeling. Cell *159*, 440–455. https://doi.org/10.1016/j.cell.2014.09.014.

17. Fomicheva, M., and Macara, I.G. (2020). Genome-wide CRISPR screen identifies noncanonical NF-kappaB signaling as a regulator of density-dependent proliferation. Elife *9*, e63603. https://doi.org/10.7554/eLife.63603.

18. Liu, Y., Yu, C., Daley, T.P., Wang, F., Cao, W.S., Bhate, S., Lin, X., Still, C., 2nd, Liu, H., Zhao, D., et al. (2018). CRISPR activation screens systematically identify factors that drive neuronal fate and reprogramming. Cell Stem Cell *23*, 758–771.e8. https://doi.org/10.1016/j.stem.2018.09.003.

19. Nuñez, J.K., Chen, J., Pommier, G.C., Cogan, J.Z., Replogle, J.M., Adriaens, C., Ramadoss, G.N., Shi, Q., Hung, K.L., Samelson, A.J., et al. (2021). Genome-wide programmable transcriptional memory by CRISPR-based epigenome editing. Cell *184*, 2503–2519.e17. https://doi.org/10.1016/j.cell.2021.03.025.

20. Okita, K., Matsumura, Y., Sato, Y., Okada, A., Morizane, A., Okamoto, S., Hong, H., Nakagawa, M., Tanabe, K., Tezuka, K.i., et al. (2011). A more efficient method to generate integration-free human iPS cells. Nat. Methods *8*, 409–412. https://doi.org/10.1038/nmeth.1591.

21. Wakao, S., Kitada, M., Kuroda, Y., Ogura, F., Murakami, T., Niwa, A., and Dezawa, M. (2012). Morphologic and gene expression criteria for identifying human induced pluripotent stem cells. PLoS One *7*, e48677. https://doi.org/10.1371/journal.pone.0048677.

22. Motomura, T., Amirneni, S., Diaz-Aragon, R., Faccioli, L.A.P., Malizio, M.R., Coard, M.C., Kocas-Kilicarslan, Z.N., Frau, C., Haep, N., Ostrowska, A., et al. (2021). Is HSD17B13 genetic variant a protector for liver dysfunction? Future perspective as a potential therapeutic target. J. Pers. Med. *11*, 619. https://doi.org/10.3390/jpm11070619.

23. Soto-Gutiérrez, A., Kobayashi, N., Rivas-Carrillo, J.D., Navarro-Alvarez, N., Zhao, D., Zhao, D., Okitsu, T., Noguchi, H., Basma, H., Tabata, Y., et al. (2006). Reversal of mouse hepatic failure using an implanted liver-assist device containing ES cell-derived hepatocytes. Nat. Biotechnol. *24*, 1412–1419. https://doi.org/10.1038/nbt1257.

24. Basma, H., Soto-Gutiérrez, A., Yannam, G.R., Liu, L., Ito, R., Yamamoto, T., Ellis, E., Carson, S.D., Sato, S., Chen, Y., et al. (2009). Differentiation and transplantation of human embryonic stem cell-derived hepatocytes. Gastroenterology *136*, 990–999. https://doi.org/10.1053/j.gastro.2008.10.047.

25. Gramignoli, R., Tahan, V., Dorko, K., Venkataramanan, R., Fox, I.J., Ellis, E.C.S., Vosough, M., and Strom, S.C. (2014). Rapid and sensitive assessment of human hepatocyte functions. Cell Transplant. *23*, 1545–1556. https://doi.org/10.3727/096368914X680064.

26. Miller, G.P., Jones, D.R., Sullivan, S.Z., Mazur, A., Owen, S.N., Mitchell, N.C., Radominska-Pandya, A., and Moran, J.H. (2009). Assessing cytochrome P450 and UDP-glucuronosyltransferase contributions to warfarin metabolism in humans. Chem. Res. Toxicol. *22*, 1239–1245. https://doi.org/10.1021/tx900031z.

27. Takebe, T., Sekine, K., Enomura, M., Koike, H., Kimura, M., Ogaeri, T., Zhang, R.R., Ueno, Y., Zheng, Y.W., Koike, N., et al. (2013). Vascularized and functional human liver from an iPSC-derived organ bud transplant. Nature *499*, 481–484. https://doi.org/10.1038/nature12271.

28. Soto-Gutierrez, A., Navarro-Alvarez, N., Yagi, H., Nahmias, Y., Yarmush, M.L., and Kobayashi, N. (2010). Engineering of an hepatic organoid to develop liver assist devices. Cell Transplant. *19*, 815–822. https://doi.org/10.3727/096368910X508933.

29. Müsch, A. (2014). The unique polarity phenotype of hepatocytes. Exp. Cell Res. *328*, 276–283. https://doi.org/10.1016/j.yexcr.2014.06.006.

30. Bhatia, S.N., Underhill, G.H., Zaret, K.S., and Fox, I.J. (2014). Cell and tissue engineering for liver disease. Sci. Transl. Med. *6*, 245sr2. https://doi.org/10.1126/scitranslmed.3005975.

31. Cohen, M., Levy, G., and Nahmias, Y. (2015). Coculture and long-term maintenance of hepatocytes. Methods Mol. Biol. *1250*, 161–173. https://doi.org/10.1007/978-1-4939-2074-7_11.

32. Michalopoulos, G.K. (2007). Liver regeneration. J. Cell. Physiol. *213*, 286–300. https://doi.org/10.1002/jcp.21172.

33. Witzigmann, D., Kulkarni, J.A., Leung, J., Chen, S., Cullis, P.R., and van der Meel, R. (2020). Lipid nanoparticle technology for therapeutic gene regulation in the liver. Adv. Drug Deliv. Rev. *159*, 344–363. https://doi.org/10.1016/j.addr.2020.06.026.

34. Maestro, S., Weber, N.D., Zabaleta, N., Aldabe, R., and Gonzalez-Aseguinolaza, G. (2021). Novel vectors and approaches for gene therapy in liver diseases. JHEP Rep. *3*,

100300. https://doi.org/10.1016/j.jhepr.2021.100300.

35. Duncan, R. (2019). Fusogenic reoviruses and their fusion-associated small transmembrane (FAST) proteins. Annu. Rev. Virol. *6*, 341–363. https://doi.org/10.1146/annurev-virology-092818-015523.

36. Takahashi, K., Tanabe, K., Ohnuki, M., Narita, M., Ichisaka, T., Tomoda, K., and Yamanaka, S. (2007). Induction of pluripotent stem cells from adult human fibroblasts by defined factors. Cell *131*, 861–872. https://doi.org/10.1016/j.cell.2007.11.019.

37. Yamanaka, S. (2020). Pluripotent stem cell-based cell therapy-promise and challenges. Cell Stem Cell *27*, 523–531. https://doi.org/10.1016/j.stem.2020.09.014.

38. Tafaleng, E.N., Malizio, M.R., Fox, I.J., and Soto-Gutierrez, A. (2021). Synthetic human livers for modeling metabolic diseases. Curr. Opin. Gastroenterol. *37*, 224–230. https://doi.org/10.1097/MOG.0000000000000726.

39. Gough, A., Soto-Gutierrez, A., Vernetti, L., Ebrahimkhani, M.R., Stern, A.M., and Taylor, D.L. (2021). Human biomimetic liver microphysiology systems in drug development and precision medicine. Nat. Rev. Gastroenterol. Hepatol. *18*, 252–268. https://doi.org/10.1038/s41575-020-00386-1.

40. Sajwan, S., and Mannervik, M. (2019). Gene activation by dCas9-CBP and the SAM system differ in target preference. Sci. Rep. *9*, 18104. https://doi.org/10.1038/s41598-019-54179-x.

41. Zhou, H., Liu, J., Zhou, C., Gao, N., Rao, Z., Li, H., Hu, X., Li, C., Yao, X., Shen, X., et al. (2018). In vivo simultaneous transcriptional activation of multiple genes in the brain using CRISPR-dCas9-activator transgenic mice. Nat. Neurosci. *21*, 440–446. https://doi.org/10.1038/s41593-017-0060-6.

42. Wu, X., Scott, D.A., Kriz, A.J., Chiu, A.C., Hsu, P.D., Dadon, D.B., Cheng, A.W., Trevino, A.E., Konermann, S., Chen, S., et al. (2014). Genome-wide binding of the CRISPR endonuclease Cas9 in mammalian cells. Nat. Biotechnol. *32*, 670–676. https://doi.org/10.1038/nbt.2889.

43. Frangoul, H., Altshuler, D., Cappellini, M.D., Chen, Y.S., Domm, J., Eustace, B.K., Foell, J., de la Fuente, J., Grupp, S., Handgretinger, R., et al. (2021). CRISPR-Cas9 gene editing for sickle cell disease and beta-thalassemia. N. Engl. J. Med. *384*, 252–260. https://doi.org/10.1056/NEJMoa2031054.

STAR★METHODS

KEY RESOURCES TABLE

REAGENT or RESOURCE	SOURCE	IDENTIFIER
Antibodies		
Mouse anti-Nanog	Cell Signaling	Cat#4893; RRID:AB_10548762
Rabbit anti-Octamer-binding transcription factor 3/4	Santa Cruz Biotechnology	Cat#sc-9081; RRID:AB_2167703
Mouse anti-Stage-specific embryonic antigen-4	BD Pharmingen	Cat#560218; RRID:AB_1645389
Mouse anti-TRA-1-60	BD Pharmingen	Cat#560173; RRID:AB_1645379
Mouse anti-Cas9	Millipore Sigma	Cat#MAC133; RRID:AB_2744694
Goat anti-SRY-Box (SOX)17	R & D Systems	Cat#NL1924R; RRID:AB_2195645
Mouse anti-α-fetoprotein	Invitrogen	Cat#180003; RRID:AB_86566
Mouse anti-Hepatocyte Nuclear Factor 4 α	Abcam	Cat#ab41898; RRID:AB_732976
Goat anti-Human Albumin	Bethyl	Cat#A80-229A; RRID:AB_67018
Rabbit anti-CD31	Abcam	Cat#ab32457; RRID:AB_726369
Rabbit anti-CYP3A4	Abcam	Cat#ab124921
Rabbit anti-UGT1A1	Abcam	Cat# ab237810
Rabbit anti-UGT1A1	Abcam	Cat# ab170858
Anti-Human Otx2 NL557-Conjugated	R&D Systems	Cat#SC022
Anti-Human SOX1 NL493-Conjugated	R&D Systems	Cat#SC022
Anti-Human Brachyury NL557-Conjugated	R&D Systems	Cat#SC022
Anti-Human HAND1 NL637-Conjugated	R&D Systems	Cat#SC022
Anti-Human GATA-4 NL493-Conjugated	R&D Systems	Cat#SC022
Anti-Human SOX17 NL637-Conjugated	R&D Systems	Cat#SC022
Mouse anti-GAPDH	Proteintech	Cat# 60004-1; RRID:AB_2107436
Rabbit anti-ACTB	Cell Signaling	Cat#4970; RRID:AB_2223172
Mouse anti-CD44	Abcam	Cat#ab6124; RRID:AB_305297
Mouse anti-αSMA	Abcam	Cat#ab7817; RRID:AB_262054
Rabbit anti-Cleaved Caspase-3	Cell Signaling	Cat#9661; RRID:AB_2341188
Mouse anti-ZO-1	Invitrogen	Cat#33-9100; RRID:AB_2533147
Rabbit anti-Integrin beta 1	Abcam	Cat#179471; RRID:AB_2773020
Biological samples		
Human adult Hepatocytes	This paper	This paper
Human fetal hepatocytes	This paper	This paper
Human fibroblast	This paper	This paper
Chemicals, peptides, and recombinant proteins		
Accutase	STEMCELL	7920
Activin A	R&D Systems	338-AC
1 X B27 without insulin supplement	Thermo Fisher Scientific	A1895601
BMP4	R&D Systems	314-BP
CELLMAXX BOVINE ALBUMIN STEM Cell Grade, Low Free Fatty Acid	Thermo Fisher Scientific	219989980
Cholesterol	Sigma Aldrich	12531-018
Collagen I, High Concentration, Rat Tail	Thermo Fisher Scientific	354249

(*Continued on next page*)

Continued

REAGENT or RESOURCE	SOURCE	IDENTIFIER
Collagenase	Sigma Aldrich	C7657
CTS KnockOut SR XenoFree Medium	Thermo Fisher Scientific	12618-012
Defined Lipid concentrate	Thermo Fisher Scientific	11905-031
DMEM, low glucose, pyruvate, HEPES	Gibco	12-320-032
DMEM, high glucose	Gibco	11-965-092
DMEM/F12, HEPES	Gibco	11-330-057
Dispase	STEMCELL	7923
Dexamethasone	Sigma Aldrich	D2915
EGM-2MV SingleQUots Kit	Lonza	CC-3202
Epidermal Growth Factor	R&D Systems	236-EG-200
FGF 2 Human	BD Biosciences	354060
GABA	Sigma Aldrich	A2129
Gentamicin	Thermo Fisher Scientific	15750060
Glutamax	Thermo Fisher Scientific	35050061
Goat Serum	Abcam	ab-7481
HCM Bullet Kit	Lonza	CC-3198
HCM SingleQuot Kit	Lonza	CC-4182
Hepatocyte Growth Factor	R&D Systems	294-HG-250
Hoechst 33342	Sigma Aldrich	B2261
Holo Transferin	CalBiochem	616424
HyClone Fetal Bovine Serum (U.S.)	Thermo Fisher Scientific	SH3007103
iCell Endothelial Cells Medium Supplement	Cellular Dynamics, Fujifilm	#R1112
Insulin	Sigma Aldrich	I9278
Insulin	Sigma Aldrich	91077C
L-Glutamine	Sigma Aldrich	G8540
Linoleic Acid	Sigma Aldrich	L1376-500MG
Lithium Chloride	Sigma Aldrich	L4408
L-pipecolic acid	Sigma Aldrich	P2519
Matrigel hESC-Qualified Matrix, LDEV-Free	Thermo Fisher Scientific	354277
Matrigel Membrane Matrix-Growth Factor Reduced	Thermo Fisher Scientific	CB-40230A
MEM Non-Essential Amino Acids Solution (100x)	Thermo Fisher Scientific	11140-050
MEM Non-Essential Amino Acids Solution (100x)	Millipore	TMS-001-C
Normal Donkey Serum	Abcam	ab-7475
Oleic Acid	Sigma Aldrich	O1008
Palmitic Acid	Sigma Aldrich	P0500
Penicillin-Streptomycin (10,000 U/ml)	Thermo Fisher Scientific	15140-122
Penicillin-Streptomycin 100x	Millipore	TMS-AB2-C
Recombinant Human Activin A	Thermo Fisher Scientific	88518
Recombinant Human Basic Fibroblast Growth Factors (bFGF)	Thermo Fisher Scientific	354060
Recombinant human basic Fibroblast Growth Factor	Lifeline Cell Technologies	61977

(*Continued on next page*)

Continued

REAGENT or RESOURCE	SOURCE	IDENTIFIER
Recombinant Human Epidermal Growth Factor (rhEGF)	Lifeline Cell Technologies	LS-1046
Rifampicin	Sigma Aldrich	R3501
RPMI1640, HEPES	Gibco	22-400-105
RT2 SYBR Green ROX qPCR Mastermix	QIAGEN	330500
TaqMan Fast Advanced Master Mix	Thermo Fisher Scientific	4444557
Trace Element B	Corning	25-022-CI
Trace Element C	Corning	25-023-CI
Transforming Growth Factor-β1	Millipore	GF111
Trypsin-EDTA (0.05%), phenol red	Sigma Aldrich	25300054
Urso deoxycolic acid	Sigma Aldrich	U5127
7-hydryoxywarfarin	Cayman	9000672
Critical commercial assays		
RT^2 Profiler™ PCR Array Human Drug Metabolism (PAHS-002ZC-6)	Qiagen	Cat#PAHS-002Z
RT^2 Profiler™ PCR Array Human Drug Metabolism: Phase II Enzymes (PAHS-069Z-6)	Qiagen	Cat# PAHS-069Z
P450-GloTM CYP3A4 Assay (Luciferin-IPA)	Promega Corporation	Cat#V9001
RNeasy mini kit	QIAGEN	Cat#74104
SuperScript III First-Strand Synthesis System	Thermo Fisher Scientific	Cat#18080-051
Experimental models: Cell lines		
Adipose-Derived mesenchymal Stem Cells; Normal, Human	American Type Culture Collection (ATCC)	PCS-500-011
Human neonatal microvascular endothelial cells	Lonza	CC-2543
HEK293-Cas9	American Type Culture Collection (ATCC)	CRL-1573Cas9
Oligonucleotides		
Octamer-binding transcription factor 4	Life Technologies	Hs04260367_gH
Nanog homeobox	Life Technologies	Hs02387400_g1
c-Myc	Life Technologies	Hs00153408_m1
Lin-28 homolog A	Life Technologies	Hs00702808_s1
SRY-Box 2	Life Technologies	Hs01053049_s1
C-X-C chemokine receptor type 4	Life Technologies	Hs00607978_s1
Forkhead box protein A1	Life Technologies	Hs04187555_m1
Forkhead box protein A2	Life Technologies	Hs00232764_m1
Hepatocyte nuclear factor 1 alpha	Life Technologies	Hs00167041_m1
Other Oligonucleotides	See Table S1	N/A
Recombinant DNA		
pCXLE-EGFP	(Okita et al., 2011)	Addgene, Cat#27082
pCXLE-hOCT3/4-shp53-F	(Okita et al., 2011)	Addgene, Cat#27077
pCXLE-hSK	(Okita et al., 2011)	Addgene, Cat#27078
pCXLE-hUL	(Okita et al., 2011)	Addgene, Cat#27080

(*Continued on next page*)

Continued

REAGENT or RESOURCE	SOURCE	IDENTIFIER
Software and algorithms		
Amaxa 4D-Nucleofector	Lonza	N/A
Image J areas quantification and Gel analysis tool	NIH	https://imagej.nih.gov/ij/
Image Lab	Bio-Rad	www.bio-rad.com/
NanoDrop	Thermo Scientific	assets.fishersci.com/
NIS-Elements AR	Nikon	www.nikoninstruments.com/
Prism 6	GraphPad	www.grapgrap.com/
StepOnePlus system	Applied Biosystems	www.thermofisher.com/
TSQ Quantum Ultra Mass Spectrometer	Thermo Scientific	www.thermofisher.com/
Other		
Haemobricks	Cellbricks	https://cellbricks.com/pages/haemobrick

RESOURCE AVAILABILITY

Lead contact

Further information and requests for resources and reagents should be directed to and will be fulfilled by the lead contact, Alejandro Soto-Gutierrez, MD, PhD (als208@pitt.edu).

Material availability

Further information and requests for resources and reagents should be directed to and will be fulfilled by the lead contact.

Data and code availability

All data produced in this study are included in the published article and its supplementary information, or are available from the lead contact upon request. This paper does not report original code. Any additional information required to reanalyze the data reported in this paper is available from the lead contact upon request.

EXPERIMENTAL MODEL AND SUBJECT DETAILS

Primary human fetal and adult hepatocytes

De-identified tissues were obtained from Magee Women's Hospital (Pittsburgh, PA) and the University of Washington Department of Pediatrics, Division of Genetic Medicine, Laboratory of Developmental Biology (Seattle, WA) after obtaining a written informed consent by a protocol approved by the Human Research Review Committee of the University of Pittsburgh (Honest broker approval number HB015 and HB000836). Human fetal hepatocytes were isolated using EMEM (Lonza, Walkersville, MD) containing 0.5 mg/mL of collagenase (Type XI, Sigma Aldrich, Saint-Louis MO, Cat. #C7657) on a lab shaker for 40 min and cultured with a DMEM medium (GIBCO, Life Technologies, Carlsbad, CA, USA) containing 1X Penicillin/Streptomycin (ThermoFisher Scientific, Waltham, MA), 10^{-7} M of insulin (Sigma-Aldrich, Saint-Louis, MO), and 5% bovine serum albumin (GIBCO, Life Technologies, Carlsbad, CA, USA). The de-identified normal human liver cells were obtained through the Liver Tissue Cell Distribution System (Pittsburgh, PA) after obtaining written informed consent. The protocol was approved by the Human Research Review Committee at the University of Pittsburgh funded by NIH Contract # HSN276201200017C. Adult human hepatocytes were also obtained from the Human Synthetic Liver Biology Core from the Pittsburgh Liver Research Center, University of Pittsburgh. The Institutional Review Board of the University of Pittsburgh has determined that the human liver cell isolation protocol employed in this study is exempt from further review. Human hepatocytes were also procured from Ira J Fox Laboratory at Children's Hospital of UPMC, after obtaining written informed consent by a protocol approved by the Human Research Review Committee and the Institutional Review Board (IRB#: PRO12090466) at the University of Pittsburgh. Specific information on age, gender, and cell viability of human liver tissue and hepatocytes used in this study is described in Table S2.

METHOD DETAILS

Production of high titer lentivirus

Lentiviral Tet-On system pcLVi(3G) was produced by Sirion-Biotech. Briefly, lentiviral HIV-based, VSVG pseudo typed, self-inactivating high titer stocks were produced by co-transfection of $1x10^6$ HEK293T cells with lentiviral packaging plasmids pRev, pMDL-GAG, and pMD2G and either the pcLVi(3G)-SAM or pcLVi(3G)-dCas9-VP64 lentiviral vectors. 48h after transfection, lentiviral particles in the culture medium were concentrated by precipitation with polyethylene glycol and dissolved in 400 µL DMEM + 10% FCS. The biological titration of each lentivirus was performed through Lenti X qRT-PCR Titration kit (Clontech). This assay measures the number of packaged lentiviral vector genomes of viral stocks. Each lentivirus yields $>1 \times 10^8$ viral particles. Each stock was preserved at −80°C.

Lentiviral transduction of human fetal fibroblasts

Primary human fetal fibroblasts were isolated by digesting the tissue in EMEM (Lonza, Walkersville, MD) containing 0.5 mg/mL of collagenase (Type XI, SigmaAldrich, Saint-Louis MO, Cat. #C7657) on a lab shaker for 40 min. Viability was assessed by trypan blue exclusion test and was routinely >85%. Fetal fibroblasts were plated at a density of $1.3x10^5$ cells/cm^2 on type I rat tail collagen-coated 12 well plates (Corning, Corning, NY). Cells were cultured and passaged 2 times to get a 100% pure population of human fetal fibroblasts, with a DMEM medium (GIBCO, Life Technologies, Carlsbad, CA, USA) containing 1X Penicillin/Streptomycin (ThermoFisher Scientific, Waltham, MA), 10^{-7} M of insulin (Sigma-Aldrich, Saint-Louis, MO), and 5% bovine serum albumin (GIBCO, Life Technologies, Carlsbad, CA, USA). Human Fetal Fibroblasts were transduced with pcLVi(3G)-dCas9-VP64 particles at an MOI of 15. The transduced cells were selected 72h after transduction with 200 µg/mL of neomycin for 21 days to generate a stable pool. The stable integration of cLVi(3G) lentiviral vectors in human fetal fibroblasts was confirmed by measuring the expression of the neomycin antibiotic cassette gene by qRT-PCR. The process was repeated using the pcLVi(3G)-SAM and the transduced cells were selected with 0.5 µg/mL of puromycin. Transduction efficiency after the selection was measured by the expression of the puromycin antibiotic cassette gene by qRT-PCR. The cell pool generated was tested for the efficiency of the Tet-On-3G system by adding 1 µg/mL of doxycycline to the cells for 48h and checking GFP expression by live fluorescence. The dCas9-VP64 and the Synergistic Activation Mediator (SAM) expression were also measured by qRT-PCR, Western Blot, and immunostaining. Quality control tests included viability, sterility (with CASO-Bouillion, Heipha), and mycoplasma testing (Lonza, Walkersville, MD).

Generation and culture of human iPSC lines

The iPSC line used was generated from human fetal fibroblast transduced with both constructions as above mentioned. Reprogramming of fetal fibroblasts was performed using episomal plasmids vectors adapted from a previously described protocol.[20] Briefly, for each nucleofection, 1 million cells were resuspended in 100 µL of the AmaxaTM NHDF Nucleofector kit (Lonza, Walkersville, MD), containing 3 ug of each of the four episomal plasmids vectors encoding OCT3/4 and p53 shRNA, SOX2 and KLF4, L-MYC and LIN28, and enhanced green fluorescent protein (eGFP) (Addgene, Boston, MA, USA). Cells were nucleofected using the Amaxa 4D-Nucleofector (Lonza, Walkersville, MD) and plated in mTeSR on human embryonic stem cell–qualified Matrigel (Corning, New York, NW)-coated plates. 2 hiPSC-$dCas9^{gain}$ colonies were isolated around 20-25 days after induction based on morphology. The presence of Tet-On-3G systems was tested in both clone cells by measuring the puromycin and neomycin antibiotic selection cassette gene expression by qPCR. Both clones were tested for their ability to induce the Tet-On-3G system by adding 1 µg/mL doxycycline and measuring either dCas9 expression by qRT-PCR and GFP expression by live fluorescence. One clone was selected, expanded for 10 passages, and tested to test the long-term efficiency of Tet-On-3G systems after multiple passages. The line was karyotyped, and pluripotency was validated by expression of NANOG, OCT4, and membrane markers SSEA and TRA160 at different passages and regularly tested negative for mycoplasma contamination.

Embryoid body formation

Embryoid bodies (EBs) cells were prepared by plating Accutase (StemCell Technologies, Vancouver, Canada) passaged iPS cells at a density of 1 to $5x10^4$ cells per cm^2 on low attachment Petri dishes for 48 hours in mTeSR. To induce differentiation, iPS cell suspensions were subsequently incubated with mTeSR supplemented with 20% FBS. EBs started to form in suspension after one week of culture. On day 20, EBs were fixed in 4% paraformaldehyde for 12 h and 70% ethanol overnight at 4°C and then embedded in paraffin,

cut sections (5-7 micron) were mounted on glass slides, for immunofluorescence using Human Three Germ Layer 3-Color Immunocytochemistry Kit (R&D Systems, Minneapolis, MN).

Cell culture

HEK293-dCas9 cells were obtained from ATCC, maintained in DMEM medium (GIBCO, Life Technologies, Carlsbad, CA, USA) supplemented with 10% HyClone fetal bovine serum (ThermoFisher Scientific, Waltham, MA), 1% Penicillin/Streptomycin (ThermoFisher Scientific, Waltham, MA) and kept at 37°C in 5% CO_2. Human fibroblasts were cultured in DMEM/F12 medium (GIBCO, Life Technologies, Carlsbad, CA, USA) supplemented with 10% HyClone fetal bovine serum (ThermoFisher Scientific, Waltham, MA), 1% Penicillin/Streptomycin (ThermoFisher Scientific, Waltham, MA), bFGF (BD, Franklin Lakes, NJ), Insulin (Sigma-Aldrich, Saint Louis, MO) and EGF (BD, Franklin Lakes, NJ) and kept at 37°C in 5% CO_2. Human mesenchymal stem cells were cultured using and following the Mesenchymal Stem Cell Growth Kit for Adipose and Umbilical-derived MSCs - Low Serum instructions (ATCC). The human vascular endothelial cells were culture using EGM^{TM}-2 Endothelial Cell Growth Medium-2 BulletKit^{TM} (Lonza, Walkersville, MD).

Differentiation of human iPSCs into hepatocytes (iHep^{gain})

Our hepatocyte differentiation protocol is summarized in Figure 2A. Human iPSCs were passaged with Accutase (StemCell Technologies, Vancouver, Canada) and re-plated at a density of 1 to 2x10^5/cm^2 at growth factor reduced Matrigel (Corning Incorporated, Corning, NY) coated plates with mTeSR. The day after, cells were exposed to a defined differentiation medium containing RPMI (Invitrogen, Carlsbad, CA), 1X B-27 w/o insulin supplement (Invitrogen, Carlsbad, CA), 0.5% Penicillin/Streptomycin (Millipore, Billerica, MA), 0.5% of Non-Essential Amino Acids (Millipore, Billerica, MA), 100 ng/mL Activin A (R&D Systems, Minneapolis, MN), 10 ng/mL BMP4 (R&D Systems, Minneapolis, MN) and 20 ng/mL FGF2 (BD, Franklin Lakes, NJ) for two days and placed in a normal O_2 incubator (Stage 1, endoderm induction). Cells were subsequently maintained in a similar medium without FGF2 and BMP4 for two days in ambient O_2/5% CO_2 incubator (Stage 2, definitive endoderm). Cells were then grown for 10 days in a defined medium containing 45% DMEM low glucose 1 g/L (ThermoFisher Scientific, Waltham, MA), 45% F-12 (ThermoFisher Scientific, Waltham, MA), 10% CTS KnockOut SR XenoFree Medium (ThermoFisher Scientific, Waltham, MA), 0.5% Non-Essential Amino Acids (ThermoFisher Scientific, Waltham, MA), 0.5% L-glutamine (ThermoFisher Scientific, Waltham, MA), 50 ng/mL HGF (R&D Systems, Minneapolis, MN) and 1% DMSO (Sigma-Aldrich, Saint Louis, MO), medium was changed every other day (Stage 3, hepatic specification). At the end of Stage 3, cells were detached and re-plated at a 30%–40% confluence in 3D sandwich culture for further maturation.

dCas9^{gain} activation and gRNA delivery in the iHep^{gain}

At the end of Stage 3 and the re-plating, cells were grown in a defined medium containing 45% DMEM low glucose 1 g/L (ThermoFisher Scientific, Waltham, MA), 45% F-12 (ThermoFisher Scientific, Waltham, MA), 10% CTS KnockOut SR XenoFree Medium, 0.5% Non-Essential Amino Acids (ThermoFisher Scientific, Waltham, MA), 0.5% L-glutamine (ThermoFisher Scientific, Waltham, MA), 0.1% of Gentamicin/Amphotericin-B (ThermoFisher Scientific, Waltham, MA), 1% of Pennicillin/Streptomycin (ThermoFisher Scientific, Waltham, MA), 50 ng/mL HGF (R&D Systems, Minneapolis, MN), 1% DMSO, 0.5 uM Dexamethasone (Sigma-Aldrich, Saint Louis, MO), 0.1% of Ascorbic Acid (Sigma-Aldrich, Saint Louis, MO), 0.1% of Bovine Serum Albumin Free of Fatty Acids, 0.1% of Hydrocortisone, 0.1% of Transferrin, 0.1% of Insulin (HCM Bullet Kit, ThermoFisher Scientific, Waltham, MA), 100 uM of Ursodeoxycolic acid (Sigma-Aldrich, Saint Louis, MO), 20 uM of Palmitic Acid (Sigma-Aldrich, Saint Louis, MO), 30 uM of Oleic Acid (Sigma-Aldrich, Saint Louis, MO), 1X of Cholesterol (ThermoFisher Scientific, Waltham, MA) and with or without 20 uM of Rifampicin (Sigma-Aldrich, Saint Louis, Missouri), accordingly with the experiment (Stage 4, hepatic maturation). At this time the cells were exposed to 1 μg/mL of doxycycline for the dCas9^{gain} activation. In the following day the cells were transduced with a gRNA pool delivered by lentivirus for the activation of CYP3A4 (gRNA1: 5′-TGGAA GAGGCTTCTCCACCT-3′ and gRNA2: 5′-ACTCAAAGGAGGTCAGTGAG-3′) or UGT1A1 (gRNA1: 5′-TGAACTCCCTGCTACCTTTG-3′; gRNA2: 5′-ATAGGCAACAACAGTTGAAC-3′ and gRNA3: 5′-ACTTTCA GAGATAAAGAAGG-3′) (Vector Builder, Chicago, IL). To enhance the transduction efficiency 8 μg/mL of Sequabrene (Sigma-Aldrich, Saint Louis, Missouri) was added in the medium and the cells were centrifuged at 300g for 1 hour at 37°C. All the construction carries an RFP protein to check transducer efficacy and an empty construction has been used as a control in some experiments (gRNA-RFP). On the following day, the medium was replaced for fresh Stage 4 medium and 48 hours later, samples were collected for further analysis or seeded into the Haemobricks (Cellbricks, Berlin, Germany) to make the Human synthetic liver^{gain} tissue.

Quantitative real-time PCR

Total RNA was isolated from human cells using RNeasy Mini kits (QIAGEN, Hilden, Germany) and reverse transcribed using SuperScript III (Invitrogen, Carlsbad, CA) following the manufacturers' instructions. We performed qPCR with a StepOnePlus system (Applied Biosystems, Foster City, CA) using TaqMan Fast Advanced Master Mix (Life Technologies, Waltham, MA). The probes used are listed in the key resources table and Table S1. Relative gene expression was normalized to β-actin (ACTB) mRNA. Relative expression was calculated using the ΔΔCT method.

Western blot

All the samples were incubated with RIPA lysis buffer (Sigma-Aldrich, Saint Louis, Missouri), 1x Halt™ Protease and Phosphatase Inhibitor Cocktail (Thermo Fisher Scientific, Waltham, MA) and incubated for 30 min at 4°C. Samples were centrifuged at 13,000g for 10 min at 4°C. The supernatant from each sample was then transferred to a new microfuge tube and was used as the whole cell lysate. Protein concentrations were determined by comparison with a known concentration of bovine serum albumin using a Pierce BCA Protein Assay Kit (ThermoFisher Scientific, Waltham, MA). 30 μg of lysate were loaded per lane into 10% Mini-PROTEAN TGX™ gel (BioRad). Next, proteins were transferred onto PVFD Transfer Membrane (Thermo Fisher Scientific, Waltham, MA). Membranes were incubated with a primary antibody solution overnight and then washed. Membranes were incubated for 1 hour in secondary antibody solution and then washed. Target antigens were finally detected using SuperSignal™ West Pico PLUS Chemiluminescent Substrate (Thermo Fisher Scientific, Waltham, MA). Images were scanned and analyzed using ImageJ software. The antibodies used are listed in the key resources table.

Immunofluorescence

Samples were washed once with PBS, fixed with 4% PFA for 15 min, and washed another 3 times with PBS. Samples were washed 3 times with wash buffer (PBS, 0.1% BSA, and 0.1% TWEEN 20) for 5 minutes and then blocked and permeabilized in blocking buffer (PBS, 10% normal donkey or goat serum, 1% BSA, 0.1% TWEEN 20, and 0.1% Triton X-100) for 1 hour at room temperature. Samples were then incubated with primary antibody in blocking buffer overnight at 4°C. Samples were washed 3 times with wash buffer for 5 minutes and incubated with secondary antibody in blocking buffer for 1 hour in the dark at room temperature. Then, the samples were washed 3 times with a wash buffer for 5 minutes, 3 times with PBS, and then counterstained with 1 μg/mL of DAPI (Sigma Aldrich) for 1 minute at room temperature in the dark. Samples were washed 3 times with PBS and stored in the dark at 4°C. Antibodies specific for antigens were acquired for immunofluorescence and list of the antibodies used can be found in key resources table. Pictures were taken using Nikon Inverted Research Fluorescence Microscope ECLIPSE Ti. Images were subsequently analyzed with ImageJ software, by generating RGB stack, pre-processed to equalize the illumination within the stack, thresholded and measured.

Transcription profiling by RT^2 profiler PCR array

RNA from Human $iHep^{gain}$ transduced with the gRNA-CYP3A4 pool exposed and no exposed to doxycycline were isolated with RNeasy Mini kits (QIAGEN, Hilden, Germany) and reverse transcribed using SuperScript III (Invitrogen, Carlsbad, CA) following the manufacturers' instructions. 84 key genes involved in the drug metabolism process were simultaneously assayed with the RT^2 Profiler PCR Array Human Drug Metabolism (PAHS-002ZC-6) (QIAGEN, Hilden, Germany) according to the manufacturer's instructions and analyzed with the Data Analysis Center (QIAGEN Hilden, Germany). The list of 84 genes analyzed can be found in Table S3.

CPY3A4 functional analysis

CYP3A4 activity was measured using P450-Glo CYP3A4 Assay (Luciferin-IPA) (Promega Corporation, Madison, WI, USA, Cat# V9001) according to the manufacturer's instructions. For induction of CYP3A4 the Human $iHep^{gain}$ was exposed to 20 uM of Rifampicin (Sigma-Aldrich, Saint Louis, Missouri) for 48 hours on the day after the gRNA-CYP3A4 lentivirus transduction. Adult human hepatocytes (HAH) were used as controls.

UGT1A1 functional analysis

The UGT1A1 gene activation was determined by mass spectroscopy. Briefly, the culture medium was supplemented with 10 μM 7-hydryoxywarfarin (Toronto Research Chemicals, Toronto, ON) for 0–48 hours. A 40 μL aliquot of the medium was collected prior to treatment and then at 6, 24, and 48 hours of treatment.

The aliquots were extracted for 7-hydroxywarfarin and 7-hydroxywarfarin glucuronide by the addition of 80 μL acetonitrile followed by 1 min of vertexing. A protein-free supernatant was collected by centrifugation in a Labnet MK-2 refrigerated centrifuge (14,000 RPM, 4°C, 5 min). The protein-free supernatant was further diluted 1:10 into acetonitrile/H_2O (20/80 v/v) for injection into the mass spectrometer. Detection was achieved in the positive mode with a ThermoFisher TSQ Quantum Ultra Mass Spectrometer, interfaced via electrospray ionization (ESI) probe with the Waters UPLC Acquity solvent delivery system. Transitions used for analysis, peak identification, and quantification of the test samples were determined by infusion and injection of pure 7-Hydroxywarfarin and the 7-Hydroxywarfarin-glucuronide (Santa Cruz Biotechnology, Dallas, TX) standards prior to sample testing. Human adult hepatocytes were used as control.

Human synthetic liver^{gain} tissue

The day after the gRNA-CYP3A4 or gRNA-UGT1A1 lentivirus transduction, the iHep^{gain} were detached and seeded into the Haemobricks (Cellbricks, Berlin, Germany) to mimic a liver tissue (representing 85%). Other support cells were also seeded into the 3D model: human vascular endothelial cells (representing 10%), human mesenchymal stem cells (representing 2.5%), and human fibroblast (representing 2.5%). 48 hours after the cell seeding, the Human synthetic liver^{gain} tissue was fixed in 4% paraformaldehyde for 12 h and 70% ethanol overnight at 4°C, and then immunolabeled. For the CYP3A4 functional analysis, 20 μM of Rifampicin (Sigma-Aldrich, Saint Louis, Missouri) was added in the medium in the day of cell seeding. After 48 hours, CYP3A4 activity was measured as previously described. To generate the 3D multicellular system, $0.25x10^6$ human iHeps^{gain} were cultured in a 24-wells low attachment plate in the presence of the LV-gRNA-CYP3A4 for 5 hours. The human vascular cells, human fibroblast, and human mesenchymal stem cells were added to the human iHep^{gain}. The system was exposed to Dox and after 4 days samples were collected for CYP3A4 protein expression and activity and fixed with 4% paraformaldehyde for 12 h and 70% ethanol overnight at 4°C. ZO-1 and ITGB1 were stained in the 3D multicellular system and human adult liver tissue.

QUANTIFICATION AND STATISTICAL ANALYSIS

Data from at least three sets of samples were used for statistical analysis. All statistical analyses were performed with Prism 6.0 Software (GraphPad Software, La Jolla, CA). All experiments were independently performed three times in triplicate. Due to the relatively small sample size, normality testing was not feasible. Data are expressed as mean ± standard deviation (SD) and were compared using an analysis of the Wilcoxon test. Values of $p < 0.05$ were considered statistically significant.